

# Robust Geodesic Regression

HA-YOUNG SHIN AND HEE-SEOK OH

Department of Statistics

Seoul National University

Seoul 08826, Korea

March 23, 2022

## Abstract

This paper studies robust regression for data on Riemannian manifolds. Geodesic regression is the generalization of linear regression to a setting with a manifold-valued dependent variable and one or more real-valued independent variables. The existing work on geodesic regression uses the sum-of-squared errors to find the solution, but as in the classical Euclidean case, the least-squares method is highly sensitive to outliers. In this paper, we use M-type estimators, including the  $L_1$ , Huber and Tukey biweight estimators, to perform robust geodesic regression, and describe how to calculate the tuning parameters for the latter two. We also show that, on compact symmetric spaces, all M-type estimators are maximum likelihood estimators, and argue for the overall superiority of the  $L_1$  estimator over the  $L_2$  and Huber estimators on high-dimensional manifolds and over the Tukey biweight estimator on compact high-dimensional manifolds. Results from numerical examples, including analysis of real neuroimaging data, demonstrate the promising empirical properties of the proposed approach.

**Keywords:** Geodesic regression; Manifold statistics; M-type estimators; Riemannian manifolds; Robust statistics.

# 1 Introduction

Much work has been done to generalize classical statistical methods for Euclidean data to manifold-valued data. Examples include principal geodesic analysis (Fletcher et al., 2004), analogous to principal component analysis, and geodesic regression (Fletcher, 2013), analogous to linear regression.

It is possible to conceptualize many types of data as lying on manifolds. Directional data in  $\mathbb{R}^3$  can be visualized as lying on  $S^2$ ; three-dimensional rotations can be represented as unit quaternions on  $S^3$ . Diffusion in the brain can be modeled by orientation distribution functions on  $S^\infty$ , which is approximated by  $S^k$  for a high value of  $k$ . The space of symmetric positive-definite (SPD) matrices has many useful applications: In neuroimaging, diffusion tensor imaging data can be modeled as  $3 \times 3$  SPD matrices (Kim et al., 2014; Zhang et al., 2019), and in computer vision, covariance matrices, which are SPD matrices, are used in appearance tracking (Cheng and Vemuri, 2013). For shape analysis, two-dimensional shape data can be represented as points on the complex projective space (Cornea et al., 2017; Fletcher, 2013), and the medial manifolds,  $M(n) = (\mathbb{R}^3 \times \mathbb{R}^+ \times S^2 \times S^2)^n$ , provide models for the shapes of organs, such as the hippocampus (Fletcher et al., 2004).

Geodesic regression, which generalizes linear regression to manifolds, has been studied in recent years (Cornea et al., 2017; Fletcher, 2013; Kim et al., 2014). In this study, we explore a new robust approach to geodesic regression that accounts for potential outliers by using M-type estimators, such as the  $L_1$ , Huber, and Tukey biweight estimators. The key step of implementing robust geodesic regression is to solve the score (estimating) equations to estimate parameters in the regression model. We propose a gradient descent algorithm to carry out robust regression on Riemannian manifolds, calculating the gradients by considering Jacobi fields for simple regression and parallel transport for multiple regression. We further show that M-type estimators are equivalent to maximum likelihood estimators on certain manifolds as a theoretical justification for the proposed method. Thus, the proposed method can be considered as an extension of M-type estimators in Euclidean space to Riemannian manifolds. In addition, we provide the theoretical values of the cutoff parameters for the

Huber and Tukey biweight functions under certain situations.

Beyond the works mentioned above, many other approaches to regression on manifolds have been proposed in the literature. Zhang et al. (2019) addressed the issue of grossly corrupted data in performing multivariate regression on manifolds. Hinkle et al. (2014) produced a framework for polynomial regression on Riemannian manifolds that provides a practical model of parametric curve regression, providing greater flexibility for geodesics. Du et al. (2014) studied geodesic regression on orientation distribution functions as elements of a Riemannian manifold. Hong et al. (2016) proposed intrinsic parametric regression on the Grassmannian manifold. As for nonparametric regression approaches for manifold-valued data, Davis et al. (2010) developed a regression analysis method of manifold-valued data using the conventional Nadaraya-Watson kernel method in terms of Fréchet expectation. Banerjee et al. (2016) presented a novel non-linear kernel-based nonparametric regression method for manifold-valued data with applications to real data collected from patients with Alzheimer’s disease and movement disorders. Steinke and Hein (2008), Hein (2009), and Steinke et al. (2010) studied nonparametric regression between Riemannian manifolds. Of particular relevance to the current study is Hein (2009), who proposed a family of robust nonparametric kernel-smoothing estimators with metric-space valued output including a robust median type estimator and the classical Fréchet mean.

The rest of this paper is organized as follows. Section 2 briefly reviews the required background knowledge of differential geometry and geodesic regression. Section 3 presents the proposed methods for robust geodesic regression and a practical algorithm. A theoretical property for M-type estimators, their cutoff parameters, and the advantages of the  $L_1$  estimator are also discussed. In Section 4, numerical experiments are presented, including simulation studies and a real data analysis of the shape of the corpus callosum in females with Alzheimer’s disease. A summary and possible avenues for future research are provided in Section 5. Section 6 explains the details of calculating the cutoff parameter for the Huber and Tukey biweight estimators, as well as the efficiency of the  $L_1$  estimator, and Appendix gives an introduction to the geometry of Kendall’s two-dimensional shape space. The data and R code used for the experiments are available at <https://github.com/hayoungshin1/Robust-Geodesic-Regression>.

## 2 Background

### 2.1 Differential Geometry Preliminaries

For a smooth manifold  $M$  and a point  $p \in M$ , the tangent space  $T_pM$  is the subspace consisting of all vectors tangent to  $M$  at  $p$ . The elements of the tangent bundle of  $M$ ,  $TM$ , take the form  $(p, v) \in M \times T_pM$ , so  $TM$  is the disjoint union of the tangent spaces of  $M$ . A Riemannian manifold  $M$  is a smooth manifold with a *Riemannian metric*; that is, a family of inner products on the tangent spaces that smoothly vary with  $p$ . This metric can be used to measure lengths on  $M$ . A geodesic between two points on  $M$  is the shortest length curve on  $M$  that connects them; in Euclidean space, geodesics are straight lines. The *geodesic* (or *Riemannian*) *distance* between two points is the length of this geodesic segment.

A geodesic  $\gamma$  is defined by its initial point,  $p = \gamma(0) \in M$  and velocity,  $v = \gamma'(0) \in T_{\gamma(0)}M$ . Then the *exponential maps*,  $\text{Exp}_p : T_pM \rightarrow M$ , are defined by  $\text{Exp}_p(v) = \gamma(1)$ , and the *logarithmic maps*,  $\text{Log}_p$ , are the inverses of the exponential maps. The exponential and logarithmic maps are analogous to vector addition and subtraction in  $\mathbb{R}^k$ . If  $q$  is in the domain of  $\text{Log}_p$ , then the geodesic distance between  $p$  and  $q$  is defined as  $d(p, q) = \|\text{Log}_p(q)\|$ . In this paper, we will denote  $\text{Exp}_p(v)$  and  $\text{Log}_p(q)$  by  $\text{Exp}(p, v)$  and  $\text{Log}(p, q)$ , respectively.

Take a differentiable curve  $\gamma : [a, b] \rightarrow M$ , not necessarily a geodesic, and a tangent vector  $v \in T_{\gamma(a)}M$ . The unique vector field  $X$  along  $\gamma$  that satisfies  $X(a) = v$  and  $\nabla_{\gamma'}X = 0$ , where  $\nabla$  is the Levi-Civita connection, is called the *parallel transport* of  $v$  along  $\gamma$ .

Given a family of geodesics  $\{\gamma_s\}$ , parametrized by and varying smoothly with respect to  $s \in \mathbb{R}$ , a Jacobi field is a vector field along the geodesic  $\gamma_0$ , and it describes how the geodesic varies at each point with respect to  $s$ ,

$$J(t) = \left. \frac{\partial \gamma_s(t)}{\partial t} \right|_{s=0}.$$

Jacobi fields satisfy a second order differential equation called the Jacobi equation, and Jacobi fields are important in the context of geodesic regression because they can be used to calculate the derivative of the exponential map. For details on the derivatives of geodesics and Jacobi fields, refer to do Carmo (1992) and Fletcher (2013).

## 2.2 Geodesic Regression

Given a dependent variable  $y$  on a Riemannian manifold  $M$  and an independent variable  $x \in \mathbb{R}$ , the simple geodesic regression model of Fletcher (2013) is

$$y = \text{Exp}(\text{Exp}(p, xv), \epsilon), \quad (1)$$

where  $p \in M$ ,  $v \in T_p M$ , and  $\epsilon \in T_{\text{Exp}(p, xv)} M$ . Kim et al. (2014) extended the simple model of (1) to a multiple regression model with several independent variables  $x^1, \dots, x^n \in \mathbb{R}$ ,

$$y = \text{Exp}\left(\text{Exp}\left(p, \sum_{j=1}^n x^j v^j\right), \epsilon\right),$$

where  $v^1, \dots, v^n \in T_p M$  and  $\epsilon$  is in the tangent space at  $\text{Exp}(p, \sum_{j=1}^n x^j v^j)$  (the superscripts are indices, not exponents). For convenience, let  $V = (v^1, \dots, v^n)$  and  $Vx := \sum_{j=1}^n x^j v^j$ . Note that we follow the notations of Fletcher (2013) and Kim et al. (2014).

Now given  $N$  data points  $(x_i, y_i) \in \mathbb{R}^n \times M$ , we define the squared loss function  $L$  by

$$L(p, v) = \sum_{i=1}^N \frac{1}{2} d(\text{Exp}(p, Vx_i), y_i)^2, \quad (2)$$

where  $d$  is the geodesic distance between points on  $M$ . Then the least-squares, or  $L_2$ , estimator  $(\hat{p}, \hat{V}) \in M \times T_p M^n$  is

$$(\hat{p}, \hat{V}) = \underset{(p, V) \in M \times T_p M^n}{\text{argmin}} L(p, V). \quad (3)$$

Unlike in the Euclidean case, the  $L_2$  estimator of (3) is generally obtained by a gradient descent algorithm because an analytical solution is typically not available. Letting  $V = 0$  in (3), the resulting  $\hat{p}$  is called the (sample) *intrinsic* (or *Karcher*) mean, and its corresponding loss is the (sample) *Fréchet* variance.

Differentiating  $L$  with respect to  $p$  and each  $v^j$  yields

$$\nabla_p L = - \sum_{i=1}^N d_p \text{Exp}(p, Vx_i)^\dagger e_i, \quad \text{and} \quad \nabla_{v^j} L = - \sum_{i=1}^N x_i^j d_{v^j} \text{Exp}(p, Vx_i)^\dagger e_i$$

for  $j = 1, \dots, n$  and  $e_i = \text{Log}(\hat{y}_i, y_i)$ . Here  $d_p \text{Exp}(p, v)$  is the derivative of the exponential map with respect to  $p$ ,  $^\dagger$  represents the adjoint operator, and  $\hat{y}_i = \text{Exp}(\hat{p}, \hat{V}x)$ . In the case of simple geodesic regression (i.e.  $n = 1$ ) on a Riemannian symmetric space (see Section 3.1), these operators can be calculated explicitly using Jacobi fields, as in Fletcher (2013). Generalizing this approach to calculate exact gradients in multiple regression models is non-trivial, but, as described in Kim et al. (2014), the gradients can be approximated well by

$$\nabla_p L \approx - \sum_{i=1}^N \Gamma_{\hat{y}_i \rightarrow p} e_i \quad \text{and} \quad \nabla_{v_j} L \approx - \sum_{i=1}^N x_i^j \Gamma_{\hat{y}_i \rightarrow p} e_i$$

where  $\Gamma_{\hat{y}_i \rightarrow p}$  denotes parallel transport of the tangent vector  $e_i$  from  $T_{\hat{y}_i} M$  to  $T_p M$  along the uniquely minimizing connecting geodesic, if it exists.

### 2.3 Variance of Tangent Bundle-valued Random Variables

Consider a tangent bundle-valued random variable  $(W_p, W_v) \in TM$ , so  $W_p \in M$ ,  $W_v \in T_{W_p} M$ . Let  $\mu_p$  be the intrinsic mean of  $W_p$ . Recalling the definition of variance in a metric space of Fréchet (1948), one can define the variance of  $W_p$  by

$$\text{Var}(W_p) := \text{E}(d(\mu_p, W_p)^2) = \text{E}(\|\text{Log}(\mu_p, W_p)\|^2). \quad (4)$$

Assuming the set of points on  $M$  for which there is not a unique minimizing geodesic connecting them to  $\mu_p$  has measure zero, we define the mean and variance of  $W_v$  as

$$\text{E}(W_v) := \text{E}(\Gamma_{W_p \rightarrow \mu_p}(W_v)) \quad \text{and} \quad \text{Var}(W_v) := \text{E}(\|\Gamma_{W_p \rightarrow \mu_p}(W_v) - \mu_v\|^2),$$

respectively, where  $\mu_v = \text{E}(W_v)$ . Given data points  $(W_{p,1}, W_{v,1}), (W_{p,2}, W_{v,2}), \dots, (W_{p,N}, W_{v,N}) \in TM$ , we call the sample intrinsic mean of the  $W_{p,i}$ ,  $\bar{W}_{p,i}$ . Fletcher et al. (2004) defined the sample variance for  $W_{p,i}$  as

$$s_p^2 := \frac{1}{N} \sum_{i=1}^N d(W_{p,i}, \bar{W}_{p,i})^2, \quad (5)$$

and we define the sample mean and sample variance for the  $W_{v,i}$  to be

$$\bar{W}_{v,i} := \frac{1}{N} \sum_{i=1}^N \Gamma_{W_{p,i} \rightarrow \bar{W}_{p,i}}(W_{v,i}) \quad \text{and} \quad s_v^2 := \frac{1}{N} \sum_{i=1}^N \|\Gamma_{W_{p,i} \rightarrow \bar{W}_{p,i}}(W_{v,i}) - \bar{W}_{v,i}\|^2, \quad (6)$$

respectively.

### 3 M-type Estimators on Riemannian Manifolds

We consider the classical linear regression model  $y = \beta_0 + \beta_1 x^1 + \dots + \beta_d x^n + \epsilon$ , where  $y \in \mathbb{R}$ , and  $\beta_0$  and  $\beta = (\beta_1, \dots, \beta_n)^T \in \mathbb{R}^n$  take the roles of  $p$  and  $V$ , respectively. The distribution of the errors  $\epsilon$  can potentially be heavy-tailed, motivating the need for a robust estimator. It is well known that the  $L_2$  estimator for  $\beta_0$  and  $\beta$  is sensitive to the presence of outliers.

To avoid this problem, one can replace the least-squares criterion by a robust M-type criterion. The robust estimate of  $(\beta_0, \beta)$  is defined as

$$(\hat{\beta}_0, \hat{\beta}) = \underset{(\beta_0, \beta)}{\operatorname{argmin}} \sum_{i=1}^N \rho(y_i - \beta_0 - x_i^T \beta)$$

for  $x_i = (x_i^1, \dots, x_i^n)^T$ , which can be found by solving

$$\sum_{i=1}^N x_i \psi(y_i - \beta_0 - x_i^T \beta) = 0,$$

where  $\psi := \rho'$ . The function  $\rho(t)$  is typically convex and symmetric about zero, quadratic in the neighborhood of zero and increasing at a rate slower than  $t^2$  for large  $t$ . The robustness comes from the fact that, compared to the squared loss,  $\rho(t)$  downweights extreme residuals. A common choice of  $\rho$  is the Huber loss function which is a continuous function constructed piecewise from quadratic and linear segments,

$$\rho_H(t) = \begin{cases} \frac{1}{2}t^2 & \text{if } |t| < c \\ c(|t| - \frac{1}{2}c) & \text{otherwise.} \end{cases}$$

Another popular loss function, the Tukey biweight function, is defined as

$$\rho_T(t) = \begin{cases} \frac{c^2}{6} \left\{ 1 - \left[ 1 - \left( \frac{t}{c} \right)^2 \right]^3 \right\} & \text{if } |t| < c \\ \frac{c^2}{6} & \text{otherwise.} \end{cases}$$

To account for possible outliers, we now consider the use of M-type estimators to estimate  $p$  and  $V$ . Generalizing from the above Euclidean setting to the manifold setting, we define a robust loss  $L_\rho$  in the mold of (2) by

$$L_\rho(p, V) = \sum_{i=1}^N \rho(d(\text{Exp}(p, Vx_i), y_i)). \quad (7)$$

Then the M-type estimator is defined as the minimizer of (7), that is,

$$(\hat{p}_\rho, \hat{V}_\rho) = \underset{(p, V) \in M \times T_p M^n}{\text{argmin}} L_\rho(p, V). \quad (8)$$

For a fixed point  $y \in M$ , the gradient is expressed as

$$\nabla_p \rho(d(y, p)) = - \frac{\rho'(\|\text{Log}(p, y)\|)}{\|\text{Log}(p, y)\|} \text{Log}(p, y),$$

so the M-type estimator is a solution to

$$\begin{aligned} \nabla_p L_\rho &= - \sum_{i=1}^N \frac{\rho'(\|e_i\|)}{\|e_i\|} d_p \text{Exp}(p, Vx_i)^\dagger e_i = 0, \\ \nabla_{v^j} L_\rho &= - \sum_{i=1}^N x_i^j \frac{\rho'(\|e_i\|)}{\|e_i\|} d_{v^j} \text{Exp}(p, Vx_i)^\dagger e_i = 0 \end{aligned}$$

for  $j = 1, \dots, n$  and  $e_i = \text{Log}(\hat{y}_i, y_i)$ . As in the least-squares case, gradients can either be calculated exactly using Jacobi fields for simple regression, or be approximated, using parallel transport, for multiple regression as

$$\nabla_p L_\rho \approx - \sum_{i=1}^N \frac{\rho'(\|e_i\|)}{\|e_i\|} \Gamma_{\hat{y}_i \rightarrow p} e_i, \quad \text{and} \quad \nabla_{v^j} L_\rho \approx - \sum_{i=1}^N x_i^j \frac{\rho'(\|e_i\|)}{\|e_i\|} \Gamma_{\hat{y}_i \rightarrow p} e_i.$$

In this study, we consider the  $L_1$  estimator with  $\rho_{L_1}(t) = |t|$ , the Huber estimator, and

the Tukey biweight estimator as robust alternatives to the least squares estimator. For the Huber and Tukey biweight estimators, it is necessary to determine the cutoff parameter  $c$ . The discussion of this topic is continued in Section 3.2.

### 3.1 M-type Estimators on Symmetric Spaces

A symmetric space is a Riemannian manifold  $M$  such that for all  $p \in M$ , there exists an involutive isometry that fixes  $p$  and reverses the geodesics that pass through  $p$ . Here, an isometry is a diffeomorphism that preserves the Riemannian distance, and an involutive isometry is an isometry that is its own inverse. The diameter of a manifold  $M$  is defined as  $\text{diam}(M) = \sup_{p_1, p_2 \in M} d(p_1, p_2)$ . One of the properties of symmetric spaces is completeness, and it is known that a complete manifold is compact if and only if it has finite diameter.

Important examples of symmetric spaces are the Euclidean spaces  $\mathbb{R}^k$ , hyperbolic spaces, the spaces of symmetric positive-definite matrices, and the cylinder  $S^1 \times \mathbb{R}$ . Examples of compact symmetric spaces include the spheres  $S^k$ , compact Lie groups, and Kendall's two-dimensional shape spaces  $\Sigma_2^K$ , which are equivalent to the complex projective spaces  $\mathbb{C}P^{K-2}$ .

For ordinary Euclidean data, some M-type estimators, such as the  $L_1$  and Huber estimators, can be expressed as maximum likelihood (ML) estimators under a certain distribution for the errors, but others, including the Tukey biweight estimator, cannot. The best known example is the  $L_2$  estimator, which is the ML estimator when the errors have a Gaussian distribution. On the other hand, on compact symmetric spaces, it can be shown that all M-type estimators of the geodesic regression model are ML estimators.

**Proposition 1.** *Let  $M$  be a compact symmetric space, with  $x_1, \dots, x_N \in \mathbb{R}^n$  and  $y_1, \dots, y_N \in M$ . Any M-estimator whose objective function satisfies  $\rho(t) > \rho(0)$ , as any reasonable objective function would, is equivalent to the maximum likelihood estimator of the geodesic regression model with  $Y$  conditionally distributed by*

$$p(y|X = x) = f(y; \text{Exp}(p, Vx), b, \rho)$$

for any  $b > 0$ , where

$$f(y; \mu, b, \rho) = \frac{1}{C(\mu, b, \rho)} \exp\left(-\frac{\rho(d(\mu, y))}{b}\right), \quad (9)$$

with

$$C(\mu, b, \rho) = \int_M \exp\left(-\frac{\rho(d(\mu, y))}{b}\right) dy. \quad (10)$$

A proof of Proposition 1 is provided in Section 6.1. In (9),  $b$  plays the role of a scale parameter. For example,  $\rho_{L_2}(x) = \frac{1}{2}x^2$  and  $b = \sigma^2$  for the  $L_2$  estimator, so the estimator is equivalent to the ML estimator of the geodesic regression model with Gaussian errors as defined in (11). We remark that this proposition is in fact true for any manifold with finite volume that is homogeneous. Another point to note is that the concept of the breakdown point is not meaningful on compact manifolds as distances between points on the manifold are bounded from above, so outliers cannot be made to be arbitrarily far away.

### 3.2 Cutoff parameters for the Huber and Tukey estimators, and efficiency of the $L_1$ estimator

For univariate Euclidean data, the cutoff parameters for the Huber and Tukey biweight estimators are typically chosen to be  $1.345\hat{\sigma}$  and  $4.685\hat{\sigma}$ , where  $\hat{\sigma} = MAD/0.6745$ ,  $MAD = \text{Median}(|e_1|, \dots, |e_N|)$  is the median absolute deviation, and  $e_i = y_i - \hat{y}_i$ . Here the value of 0.6745 is chosen because, for  $X \sim N(\mu, \sigma^2)$ ,  $Pr(|X - \mu| < 0.6745\sigma) = 1/2$ , and the values of 1.345 and 4.685 are chosen so that, given i.i.d  $X_i \sim N(\mu, \sigma^2)$ ,  $i = 1, \dots, N$ , the asymptotic relative efficiency (ARE) of the sample M-type estimator for  $\mu$ ,  $\hat{X}$ , to the least-squares estimator, the sample mean  $\bar{X}$ , is 95% (i.e.,  $\lim_{N \rightarrow \infty} [\text{Var}(\bar{X})/\text{Var}(\hat{X})] = 0.95$ ). By analogy, determining the cutoff parameter  $c$  for the Huber and Tukey biweight estimators on a symmetric space also requires two steps: (a) estimating  $\sigma$  by  $MAD/\xi$ , and (b) finding the multiple of  $\sigma$  that would give an ARE of the M-type estimator of location to the sample intrinsic mean of 95% under a Gaussian distribution. In the manifold case,  $MAD = \text{Median}(\|e_1\|, \dots, \|e_N\|)$ , with  $e_i = \text{Log}(\text{Exp}(p, x_i v), y_i)$ , and we have defined the variance of a manifold-valued random variable as in (4) and the relative efficiency as the ratio of two variances, as in the univariate Euclidean case.

The Gaussian distribution, as defined in Fletcher (2013), on a  $k$ -dimensional connected manifold  $M$  has the following density

$$f(y; \mu, \sigma^2) = \frac{1}{C(\mu, \sigma^2)} \exp\left(-\frac{d(y, \mu)^2}{2\sigma^2}\right), \quad (11)$$

where

$$C(\mu, \sigma^2) = \int_M \exp\left(-\frac{d(y, \mu)^2}{2\sigma^2}\right) dy.$$

Given i.i.d  $Y_i$ ,  $i = 1, \dots, N$ , distributed according to (11), we approximate the M-type estimator  $\hat{Y}$  on the manifold by  $\text{Exp}(\mu, \hat{Y}^*)$ , where  $\hat{Y}^*$  is the M-type estimator for the points  $Y_i^* := \text{Log}(\mu, Y_i)$  in the tangent space at  $\mu$ . As the tangent space is isomorphic to  $\mathbb{R}^k$ , we treat these points as belonging to  $\mathbb{R}^k$  and consider the  $Y_i^*$  to be distributed according to an isotropic multivariate Gaussian distribution with mean 0 and variance  $\sigma^2 I_k$ . That is, letting  $\sigma = 1$  without loss of generality, the density of  $Y_i^*$  is given by  $f(y) = \phi_k(y)$  for  $y \in \mathbb{R}^k$ , where  $Z_k \sim N_k(0, I_k)$  is the standard  $k$ -variate Gaussian random variable and  $\phi_k = (2\pi)^{-\frac{k}{2}} \exp(-\sum_{j=1}^k (y^j)^2)$  is its density. Here  $y^j$  denotes the  $j$ th coordinate of  $y$ , not the  $j$ th power of  $y$ . These approximations are reasonable for small  $\sigma$ . We will also assume  $k \geq 2$ ; the numbers when  $k = 1$ , provided in Table 1, are already well known.

The calculations involved in determining the  $c$  values are very tedious and lengthy; for details, refer to Section 6.2. Because of the aforementioned tangent space approximation, these results are exact when  $M = \mathbb{R}^k$ . Ultimately, the value of the constant  $\xi$  in  $MAD/\xi$  is

$$\xi = \sqrt{2P^{-1}\left(\frac{k}{2}, \frac{1}{2}\right)}, \quad (12)$$

where  $P^{-1}(a, z)$  is the inverse of the lower regularized gamma function  $P(a, z) := \gamma(a, z)/\Gamma(z)$ ,  $\Gamma(z)$  is the gamma function, and  $\gamma(a, z)$  is the lower incomplete gamma function. In addition, the approximate AREs of the sample Huber and Tukey biweight estimators to the sample

mean are, respectively,

$$\text{ARE}_{H,L_2}(c, k) \approx A_H(c, k) := \frac{\left\{ \frac{k}{2} \gamma\left(\frac{k}{2}, \frac{c^2}{2}\right) + 2^{-\frac{3}{2}} c(k-1) \Gamma\left(\frac{k-1}{2}, \frac{c^2}{2}\right) \right\}^2}{\Gamma\left(\frac{k+2}{2}\right) \left\{ \gamma\left(\frac{k+2}{2}, \frac{c^2}{2}\right) + \frac{c^2}{2} \Gamma\left(\frac{k}{2}, \frac{c^2}{2}\right) \right\}}, \quad (13)$$

and

$$\text{ARE}_{T,L_2}(c, k) \approx A_T(c, k) := \frac{\left\{ \frac{2(k+4)}{c^4} \gamma\left(\frac{k+4}{2}, \frac{c^2}{2}\right) - \frac{2(k+2)}{c^2} \gamma\left(\frac{k+2}{2}, \frac{c^2}{2}\right) + \frac{k}{2} \gamma\left(\frac{k}{2}, \frac{c^2}{2}\right) \right\}^2}{\Gamma\left(\frac{k+2}{2}\right) \left\{ \gamma\left(\frac{k+2}{2}, \frac{c^2}{2}\right) - \frac{8}{c^2} \gamma\left(\frac{k+4}{2}, \frac{c^2}{2}\right) + \frac{24}{c^4} \gamma\left(\frac{k+6}{2}, \frac{c^2}{2}\right) - \frac{32}{c^6} \gamma\left(\frac{k+8}{2}, \frac{c^2}{2}\right) + \frac{16}{c^8} \gamma\left(\frac{k+10}{2}, \frac{c^2}{2}\right) \right\}}, \quad (14)$$

where  $c$  is the cutoff parameter and  $\Gamma(a, z)$  is the upper incomplete gamma function. Note that these two equations assume without loss of generality that  $\sigma = 1$ . Finally, we calculate the partial derivatives of (13) and (14) with respect to  $c$ , and then use the Newton-Raphson method to find  $c_H$  and  $c_T$ , the values of  $c$  for which the approximate  $\text{ARE}_{H,L_2}$  and  $\text{ARE}_{T,L_2}$ , respectively, are 95%.

Note that  $\lim_{c \rightarrow 0} \text{ARE}_{H,L_2}(c, k) = \text{ARE}_{L_1,L_2}(k)$ . Several properties of  $A_{L_1}$ , the approximate ARE of the  $L_1$  estimator to the  $L_2$  estimator calculated by letting  $c \rightarrow 0$  for  $A_H$  in (13), are given in the following proposition.

**Proposition 2.** (a) Defining  $A_H(c, k)$  as in (13), it follows that

$$\text{ARE}_{L_1,L_2}(k) \approx \lim_{c \rightarrow 0} A_H(c, k) = A_{L_1}(k) := \frac{\Gamma^2\left(\frac{k+1}{2}\right)}{\Gamma\left(\frac{k}{2}\right) \Gamma\left(\frac{k+2}{2}\right)}. \quad (15)$$

(b)  $A_{L_1}(k)$ , as defined in (15), is increasing in  $k \in \mathbb{Z}^+$ . (c)  $\lim_{k \rightarrow \infty} A_{L_1}(k) = 1$ .

A proof of Proposition 2 is provided in Section 6.3. When  $k = 10$ , the approximate  $\text{ARE}_{L_1,L_2}$  is 0.95131, over 95%. So in higher dimensions, the Huber estimator becomes unnecessary as the  $L_1$  estimator is sufficiently efficient, and in very high-dimensional cases, even the  $L_2$  estimator becomes unnecessary. The usual reasons for favoring the  $L_2$  in the univariate Euclidean case are efficiency and ease of computation, but as Proposition 2 shows, on high-dimensional manifolds the improvement in efficiency from using the  $L_2$  over the  $L_1$  estimator is

negligible even with Gaussian errors. For example, the approximate ARE  $A_{L_1}(50) = 0.99005$ , over 99%. Regarding computation, the geodesic regression problem is solved with a gradient descent algorithm regardless of choice of estimator, so this disadvantage of the  $L_1$  estimator is also mitigated. On the other hand, the  $L_1$  estimator is clearly more robust than the  $L_2$  estimator. We thus argue that the use of the  $L_2$  estimator should be superseded by that of the  $L_1$  estimator on high-dimensional manifolds.

With respect to the Tukey biweight estimator, the  $L_1$  estimator is not preferred in the univariate Euclidean case, again due to a lack of efficiency, difficulty of computation, and also a low breakdown point. As before, efficiency and computation are no longer issues on high-dimensional manifolds, and in fact the  $L_1$  estimator may even be more efficient. Additionally, if the diameter of the manifold is finite, the breakdown point is rendered moot, as was noted at the end of Section 3.1. Therefore, one might prefer the  $L_1$  estimator over the Tukey biweight estimator on compact high-dimensional manifolds.

Table 1 gives the values of  $\xi$  of (12), and the cutoff parameters for the Huber and Tukey biweight estimators  $c_H$  and  $c_T$ , which are the multiples of  $\hat{\sigma}$  for these estimators, respectively, for  $k = 1, 2, 3, 4, 5, 6$  in  $\mathbb{R}^k$ . We also include the approximate  $ARE_{L_1, L_2}$ , which in lower dimensions rapidly improves as  $k$  increases.

**Table 1:**  $\xi$ ,  $c_H$  and  $c_B$  according to  $k = 1, \dots, 6$ .

$k$	1	2	3	4	5	6
$\xi$	0.67449	1.17741	1.53817	1.83213	2.08601	2.31260
$c_H$	1.34500	1.50114	1.62799	1.73107	1.81202	1.86934
$c_T$	4.68506	5.12299	5.49025	5.81032	6.09627	6.35622
$A_{L_1}$	0.63662	0.78540	0.84883	0.88357	0.90541	0.92039

Even though the formulae in this section are calculated under the assumption that  $k \geq 2$ , (12), (14), and (15) happen to still be valid when  $k = 1$ , producing the figures in the  $k = 1$  column of Table 1, as are Proposition 2(a) and 2(b). The approximate ARE in (13) can also be adjusted to work by removing the second summand in the curly brackets of the numerator.

### 3.3 Implementation for M-type Estimators on Riemannian Manifolds

Here we discuss the implementation of the proposed M-type estimator on Riemannian manifolds. The gradient descent algorithm to find the solution of the robust geodesic regression problem in (8) is outlined in Algorithm 1 below.

We remark that  $\nabla_p L_\rho$  and  $\nabla_V L_\rho$  in lines 14, 15, 16, and 28 are calculated exactly using Jacobi fields in the case of simple regression and approximately using parallel transport in the case of multiple regression;  $L_\rho$  is defined as in (7). The purpose of  $\lambda_{\max}/\|\nabla_p L_\rho\|$  in lines 14 and 28 are to prevent the steps for  $p$ ,  $-\lambda\nabla_p L_\rho$ , from getting too large.

## 4 Numerical Experiments

### 4.1 Simulations on $S^k$

The  $k$ -spheres  $S^k$  are useful manifolds with many applications, several of which are mentioned in Section 1. Here we evaluate the efficacy of the proposed M-type estimators for simple geodesic regression on  $S^2$  and multiple geodesic regression on  $S^3$  using simulated data.

Before presenting the simulation setup, we discuss some background information on  $S^k$ . The exponential map for  $S^k$  is given by

$$\text{Exp}(p, v) = \cos(\|v\|)p + \sin(\|v\|)\frac{v}{\|v\|}$$

for  $p \in S^k$ ,  $v \in T_p S^k$ . For  $p, q \in S^k$ ,  $p \neq -q$ , the logarithmic map is given by

$$\text{Log}(p, q) = \cos^{-1}(\langle p, q \rangle) \frac{q - \langle p, q \rangle p}{\|q - \langle p, q \rangle p\|},$$

and the parallel transport of a vector  $v \in T_p S^n$  along the unique minimizing geodesic from  $p$  to  $q$  (provided  $q \neq -p$ ) is given by

$$\Gamma_{p \rightarrow q}(v) = v^\perp + \|v^\top\| \left( \cos(\|\text{Log}(p, q)\|) \frac{\text{Log}(p, q)}{\|\text{Log}(p, q)\|} - \sin(\|\text{Log}(p, q)\|) p \right),$$

---

**Algorithm 1** Gradient descent algorithm for geodesic regression

---

```
1: Input:  $x_1, \dots, x_N \in \mathbb{R}^n$ ,  $y_1, \dots, y_N \in M$  for  $k$ -dimensional  $M$  and  $\rho : \mathbb{R} \rightarrow \mathbb{R}^+$ .
2: Output:  $p \in M, V \in T_p M^n$ 
3: Initialize  $p$  as the intrinsic mean of  $\{y_1, \dots, y_N\}$ ,  $V$  as 0, and  $\lambda_{max}$ , and center  $x$ .
4: if  $\rho = \rho_H$  or  $\rho_B$  then
5:   Calculate  $\xi$  using (12).
6:   for  $i$  in 1 to  $N$  do
7:      $e_i = \text{Log}(\text{Exp}(p, Vx_i), y_i)$ 
8:   end for
9:    $MAD = \text{Median}(\|e_1\|, \dots, \|e_N\|)$ 
10:  Calculate  $c_H$  or  $c_B$  using Newton-Raphson's method on (13) or (14), respectively.
11:   $\hat{\sigma} = MAD/\xi$ 
12:   $c = c_H \hat{\sigma}$  or  $c = c_H \hat{\sigma}$ .
13: end if
14:  $\lambda = \min(0.1, \lambda_{max}/\|\nabla_p L_\rho\|)$ 
15: while termination condition do
16:    $p_{new} = \text{Exp}(p, -\lambda \nabla_p L_\rho)$ 
17:    $V_{new} = \Gamma_{p \rightarrow p_{new}}(V - \lambda \nabla_V L_\rho)$ 
18:   if  $E_\rho(p, V) \geq E_\rho(p_{new}, V_{new})$  then
19:      $p = p_{new}$  and  $V = V_{new}$ 
20:     if  $\rho = \rho_H$  or  $\rho_B$  then
21:       for  $i$  in 1 to  $N$  do
22:          $e_i = \text{Log}(\text{Exp}(p, Vx_i), y_i)$ 
23:       end for
24:        $MAD = \text{Median}(\|e_1\|, \dots, \|e_N\|)$ 
25:        $\hat{\sigma} = MAD/\xi$ 
26:        $c = c_H \hat{\sigma}$  or  $c = c_H \hat{\sigma}$ 
27:     end if
28:      $\lambda = \min(2\lambda, \lambda_{max}/\|\nabla_p L_\rho\|)$ 
29:   else
30:      $\lambda = \lambda/2$ 
31:   end if
32: end while
```

---

where

$$v^\top = \left\langle v, \frac{\text{Log}(p, q)}{\|\text{Log}(p, q)\|} \right\rangle \frac{\text{Log}(p, q)}{\|\text{Log}(p, q)\|}, \text{ and } v^\perp = v - v^\top,$$

which denote the parts of  $v$  that are parallel and orthogonal to  $\text{Log}(p, q)$ , respectively. In the simple regression case, the exact gradients with respect to  $p$  and  $v$ , calculated using Jacobi

fields, are

$$\begin{aligned}
\nabla_p E_\rho &= - \sum_{i=1}^N \frac{\rho'(\|e_i\|)}{\|e_i\|} d_p \text{Exp}(p, x_i v)^\dagger e_i \\
&= - \sum_{i=1}^N \frac{\rho'(\|e_i\|)}{\|e_i\|} \left( \cos(\|x_i v\|) \Gamma_{\hat{y}_i \rightarrow p}^\perp(e_i) + \Gamma_{\hat{y}_i \rightarrow p}^\top(e_i) \right), \text{ and} \\
\nabla_v E_\rho &= - \sum_{i=1}^N x_i \frac{\rho'(\|e_i\|)}{\|e_i\|} d_v \text{Exp}(p, x_i v)^\dagger e_i \\
&= - \sum_{i=1}^N x_i \frac{\rho'(\|e_i\|)}{\|e_i\|} \left( \frac{\sin(\|x_i v\|)}{\|x_i v\|} \Gamma_{\hat{y}_i \rightarrow p}^\perp(e_i) + \Gamma_{\hat{y}_i \rightarrow p}^\top(e_i) \right),
\end{aligned}$$

where  $e_i = \text{Log}(\hat{y}_i, y_i)$ , and  $\Gamma_{\hat{y}_i \rightarrow p}^\top(e_i)$  and  $\Gamma_{\hat{y}_i \rightarrow p}^\perp(e_i)$  are defined by

$$\Gamma_{\hat{y}_i \rightarrow p}^\top(e_i) = \left\langle \Gamma_{\hat{y}_i \rightarrow p}(e_i), \frac{v}{\|v\|} \right\rangle \frac{v}{\|v\|}, \text{ and } \Gamma_{\hat{y}_i \rightarrow p}^\perp(e_i) = \Gamma_{\hat{y}_i \rightarrow p}(e_i) - \Gamma_{\hat{y}_i \rightarrow p}^\top(e_i)^\top.$$

For more information on how to calculate the Jacobi fields and use them to derive the exact gradients of exponential maps, see Fletcher (2013).

The experimental setup is similar, but not identical, to the one used in Fletcher (2013). The parameters for the simple regression model on  $S^2$  are set to  $p = (1, 0, 0)$ ,  $v^1 = (0, \pi/4, 0)$ . For the multiple regression model on  $S^3$ , the parameters are set to  $p = (1, 0, 0, 0)$ ,  $v^1 = (0, \pi/4, 0, 0)$ , and  $v^2 = (0, 0, 0, -\pi/6)$ . Several different sample sizes are considered:  $N = 2^h$  for  $h = 2, 3, \dots, 8$ . The  $x_i$  are generated from the uniform distribution on  $[-1/2, 1/2]$ . Three different types of noise are considered as follows:

- **G**: an isotropic multivariate Gaussian distribution in the tangent space with  $\sigma = \pi/8$  and  $\Sigma = \sigma^2 I_k$ ,
- **T**: a multivariate  $t$ -distribution in the tangent space with  $\Sigma = (\pi/16)^2 I_k$  and  $\nu = 3$ , and
- **C**: a contaminated Gaussian mixture distribution, that is, a mixture of two isotropic multivariate Gaussian distribution, one with  $\Sigma = (\pi/24)^2 I_k$  and a probability of 0.9, the other with  $\Sigma = (\pi/6)^2 I_k$  and a probability of 0.1.

Note that as  $\sigma$  is small, type G approximates the distribution induced by the Gaussian

distribution on the manifold itself very well. The distributions in scenarios T and C are useful for examining robustness as they have heavier tails than the Gaussian distribution, producing outliers.

We set the  $\xi$ ,  $c_H$ , and  $c_T$  values from Section 3.2, calculated to give an asymptotic efficiency of 95% relative to the  $L_2$  estimator, to 1.17741, 1.50114, and 5.12299, respectively, on  $S_2$ . On  $S_3$ , we used 1.53817, 1.62799, and 5.49025, respectively.

For each  $h$ ,  $L = 1024$  datasets are simulated. Then for each simulated set, four regression estimates are obtained by applying the  $L_2$ ,  $L_1$ , Huber, and Tukey biweight estimators. For evaluation, we utilize the mean squared errors (MSE) for  $\hat{p}$  and each  $\hat{v}^j$ , defined as

$$\text{MSE}(\hat{p}) := \frac{1}{L} \sum_{\ell=1}^L d(\hat{p}_\ell, p)^2, \quad \text{and} \quad \text{MSE}(\hat{v}^j) := \frac{1}{L} \sum_{\ell=1}^L \|\Gamma_{\hat{p}_\ell \rightarrow p}(\hat{v}_\ell^j) - v^j\|^2, \quad (16)$$

where  $\hat{p}_\ell$  and  $\hat{v}_\ell^j$  are the estimates for  $p$  and  $v^j$  from the  $\ell$ th trial.

Figure 1 shows the results. In every case, the MSEs all approached zero as sample size increases. We focus on the experiments in which the sample size is reasonably large (at least  $2^3 = 8$  or  $2^4 = 16$ ). The least-squares  $L_2$  estimator performed the best for the Gaussian errors G, but the Huber and Tukey biweight estimators are almost as good. On  $S^3$ , even the  $L_1$  estimator does not perform significantly worse than the other three estimators, reflecting the fairly high (approximate) efficiency of 0.84883 in Table 1. For the noise data T, the  $L_2$  estimator performs very poorly, while the other three have almost identical MSE values on both  $S^2$  and  $S^3$ , though generally the Tukey biweight estimator slightly better, followed by the  $L_1$  estimator, and then the Huber estimator. For the contaminated mixture case C, the estimators, in order from worst to best, are the  $L_2$ ,  $L_1$ , Huber, and Tukey biweight estimators, with the latter two being very close. The  $L_2$  estimator is completely outclassed. When  $N$  was small ( $N = 2^2 = 4$  or  $2^3 = 8$ ), the  $L_1$  estimator outperforms the others, significantly so in the  $S^3$  experiments, regardless of the distribution of the errors.

In the G case, we also use (5) to calculate the sample variances  $s_{p,L_2}^2$ ,  $s_{p,L_1}^2$ ,  $s_{p,H}^2$ , and  $s_{p,T}^2$  of the  $p$  estimates and (6) for the sample variances  $s_{v^j,L_2}^2$ ,  $s_{v^j,L_1}^2$ ,  $s_{v^j,H}^2$ , and  $s_{v^j,T}^2$  of the  $v^j$  estimates, for the  $L_2$ ,  $L_1$ , Huber and Tukey biweight estimators, respectively. We calculate

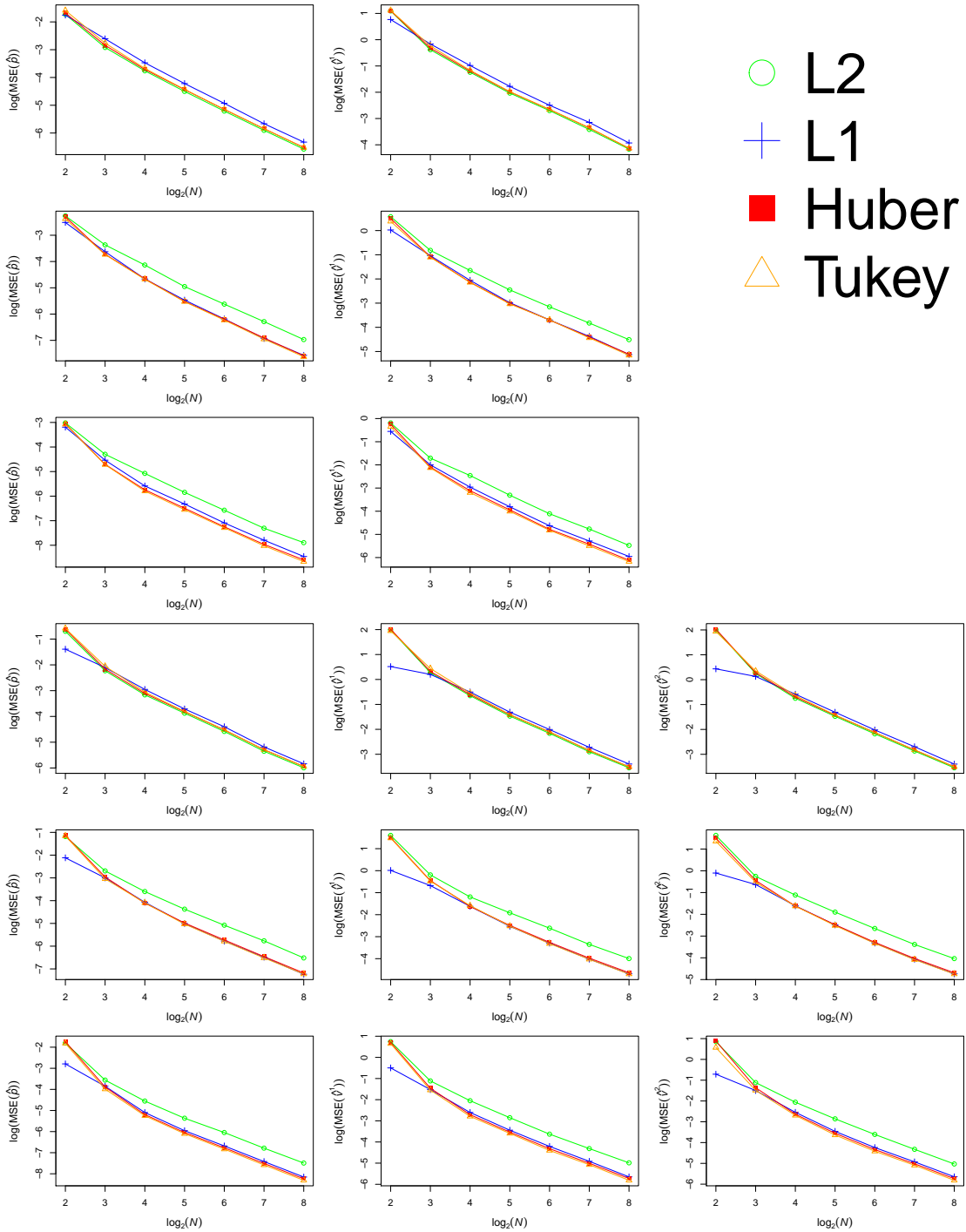


**Figure 1:** The effect of sample size,  $N$ , on various MSEs estimated from synthetic data. Both axes use logarithmic scales. The first three rows show the results on  $S^2$ ; the last three rows show the results on  $S^3$ . The errors are type G in the first and fourth rows, type T in the second and fifth and type C in the third and sixth.

the relevant sample relative efficiencies by taking the appropriate ratios. Tables 2 and 3 display these results. These figures match closely with our expectations of an ARE to the  $L_2$  estimator of 95% for the Huber and Tukey biweight estimators, and 78.54% and 84.88% on  $S^2$  and  $S^3$ , respectively, for the  $L_1$  estimator, as listed in Table 1. Assuming the parameter estimates are unbiased, a comparison of (16) to (5) and (6) shows that the MSEs in the first and fourth rows of Figure 1 can also have been used to compute the relative efficiencies in these tables.

**Table 2:** Relative efficiencies of the three robust estimators to the  $L_2$  estimator in the G case on  $S^2$ .

$\log_2(N)$	2	3	4	5	6	7	8
$s_{p,L_2}^2/s_{p,L_1}^2$	1.0263610	0.7315716	0.7485509	0.7537326	0.7565859	0.7886033	0.7780410
$s_{p,L_2}^2/s_{p,H}^2$	0.9545316	0.9250899	0.9520053	0.9382755	0.9434537	0.9441408	0.9430704
$s_{p,L_2}^2/s_{p,T}^2$	0.8688929	0.8541114	0.9176730	0.9285858	0.9373870	0.9443081	0.9454206
$s_{v^1,L_2}^2/s_{p,L_1}^2$	1.4053354	0.8086485	0.7744326	0.7735143	0.8166613	0.7646757	0.7920269
$s_{v^1,L_2}^2/s_{p,H}^2$	0.9941910	0.9419032	0.9543974	0.9551271	0.9570937	0.9427577	0.9688966
$s_{v^1,L_2}^2/s_{p,T}^2$	0.9839447	0.8670442	0.9259160	0.9456212	0.9588183	0.9377588	0.9702942

**Table 3:** Relative efficiencies of the three robust estimators to the  $L_2$  estimator in the G case on  $S^3$ .

$\log_2(N)$	2	3	4	5	6	7	8
$s_{p,L_2}^2/s_{p,L_1}^2$	2.0018028	0.8823905	0.8096156	0.8483667	0.8330429	0.8456351	0.8565228
$s_{p,L_2}^2/s_{p,H}^2$	0.9221662	0.9397125	0.9467181	0.9475339	0.9459580	0.9420096	0.9493195
$s_{p,L_2}^2/s_{p,T}^2$	0.8936785	0.8414880	0.8979819	0.9346504	0.9373267	0.9409227	0.9492401
$s_{v^1,L_2}^2/s_{p,L_1}^2$	4.6023087	1.0839885	0.8654657	0.8526543	0.8577878	0.8378540	0.8596134
$s_{v^1,L_2}^2/s_{p,H}^2$	0.9789346	0.9534018	0.9561830	0.9489850	0.9488152	0.9514822	0.9606819
$s_{v^1,L_2}^2/s_{p,T}^2$	1.0504359	0.8503392	0.9032767	0.9370882	0.9454196	0.9465263	0.9572580
$s_{v^2,L_2}^2/s_{p,L_1}^2$	4.9555685	1.1328630	0.8497212	0.8481885	0.8544510	0.8401306	0.8611429
$s_{v^2,L_2}^2/s_{p,H}^2$	0.9764562	0.9700910	0.9508238	0.9584123	0.9489881	0.9583070	0.9601424
$s_{v^2,L_2}^2/s_{p,T}^2$	1.0699764	0.9036769	0.8978617	0.9470666	0.9461826	0.9556484	0.9582522

Figure 2 shows an example simulation for each of the G, T, and C scenarios. Figures 2b and 2c, in which the presence of outliers is clearly visible, illustrate the superior robustness properties of the other three estimators over the  $L_2$  estimator, while Figure 2a demonstrates that even in the Gaussian case, the Huber and Tukey biweight estimators, in contrast to the  $L_1$  estimator, do not perform significantly worse than the  $L_2$  estimator.

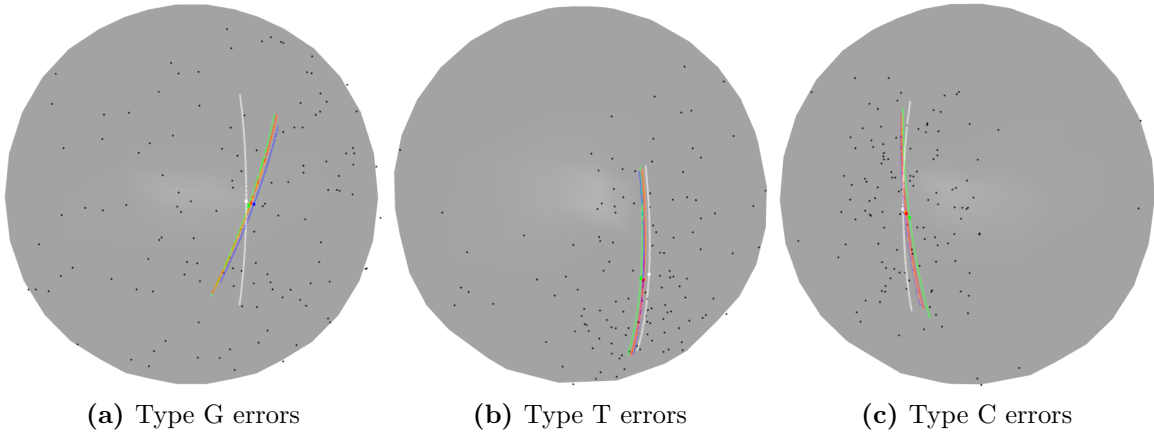


**Figure 2:** Examples of simulations in the simple regression case on  $S^2$  using different types of noise. The sample size is  $2^7 = 128$  and the small black dots are the  $y_i$ . The images each show 5 geodesics from  $\gamma(-\frac{1}{2})$  to  $\gamma(\frac{1}{2})$ ; that is, from  $\text{Exp}(p, -\frac{1}{2}v)$  to  $\text{Exp}(p, \frac{1}{2}v)$ .  $\gamma(0)$ , or  $p$ , is indicated by a large dot. The true geodesics are white, the  $L_2$  solutions are green, the  $L_1$  solutions blue, the Huber solutions red and the Tukey biweight solutions orange. We can evaluate the performance of each estimator by comparing the regression results to the true geodesics.

## 4.2 Real Data Analysis: Corpus Callosum Shape Data

Mathematically, a shape refers to the geometry of an object after translation, scaling, and rotation have been removed. Kendall's two-dimensional shape space  $\Sigma_2^K$  is the set of two-dimensional  $K$ -gon shapes, that is, the set of all possible non-coincident  $K$ -configurations in the two-dimensional plane modulo translation, scaling, and rotation, and is a compact symmetric space. For details on the structure of  $\Sigma_2^K$ , including the exponential and logarithmic maps, parallel transport and Jacobi field equations, refer to Appendix.

The corpus callosum, the largest white matter structure in the human brain, is a major nerve tract that connects the two cerebral hemispheres, facilitating interhemispheric communication. In this section, we perform simple geodesic regression with M-type estimators to analyze the relationship between the shape of the corpus callosum and age in older females with Alzheimer's disease (AD). We have used the preprocessed data provided by Cornea et al. (2017) on their website <http://www.bios.unc.edu/research/bias/software.html>. The planar shape data, obtained from the mid-sagittal slices of magnetic resonance images (MRI), are from the Alzheimer's disease neuroimaging initiative (ADNI) study. As mentioned above, the 88 female subjects with AD, whose ages range from 55 to 92, are the focus of this analy-

sis, though the dataset contains data for both males and females with and without AD. Each shape is extracted from the MRI and segmented using the `FreeSurfer` and `CCseg` packages, resulting in a 50-by-2 matrix. The rows of this matrix give the planar coordinates of  $K = 50$  landmark points on the boundary of the shape, with enforced correspondences between the landmarks of different subjects.

Because the real dimension of the manifold is  $2K - 4 = 96 \geq 10$ , the  $L_1$  estimator is already efficient enough to make the Huber estimator unnecessary. Indeed, under the Euclidean, tangent space approximation,  $\text{ARE}_{L_1, L_2} = 0.99481$ . Therefore, we have only used the  $L_2$ ,  $L_1$ , and Tukey biweight estimators to analyze this dataset. Using (12) and (14), we calculated  $\xi$  and  $c_T$  to be 9.76392 and 14.72356, respectively. Geodesic regression is carried out six times. First, we apply the three estimators to the original data, giving  $(\hat{p}_{L_2}, \hat{v}_{L_2})$ ,  $(\hat{p}_{L_1}, \hat{v}_{L_1})$ , and  $(\hat{p}_T, \hat{v}_T)$ ; we use  $(\hat{p}_{L_2}, \hat{v}_{L_2})$  as the baseline for comparison. Then we intentionally generate outliers by tampering with the data: for 20 of the 88 subjects, the shapes of their corpus callosums are flipped (reflected shapes are not considered equivalent in Kendall’s shape space, for good reason). The three estimators are applied to this tampered dataset, resulting in  $(\hat{p}'_{L_2}, \hat{v}'_{L_2})$ ,  $(\hat{p}'_{L_1}, \hat{v}'_{L_1})$ , and  $(\hat{p}'_T, \hat{v}'_T)$ .

**Table 4:** Comparing the various regression parameter estimates against  $(\hat{p}_{L_2}, \hat{v}_{L_2})$ .

$d_{\Sigma_2^{50}}(\hat{p}_{L_1}, \hat{p}_{L_2})$	0.0018924	$\ \Gamma_{\hat{p}_{L_1} \rightarrow \hat{p}_{L_2}}(\hat{v}_{L_1}) - \hat{v}_{L_2}\ $	0.0002177
$d_{\Sigma_2^{50}}(\hat{p}_T, \hat{p}_{L_2})$	0.0061325	$\ \Gamma_{\hat{p}_T \rightarrow \hat{p}_{L_2}}(\hat{v}_T) - \hat{v}_{L_2}\ $	0.0011544
$d_{\Sigma_2^{50}}(\hat{p}'_{L_2}, \hat{p}_{L_2})$	0.1444551	$\ \Gamma_{\hat{p}'_{L_2} \rightarrow \hat{p}_{L_2}}(\hat{v}'_{L_2}) - \hat{v}_{L_2}\ $	0.0051700
$d_{\Sigma_2^{50}}(\hat{p}'_{L_1}, \hat{p}_{L_2})$	0.0182806	$\ \Gamma_{\hat{p}'_{L_1} \rightarrow \hat{p}_{L_2}}(\hat{v}'_{L_1}) - \hat{v}_{L_2}\ $	0.0009981
$d_{\Sigma_2^{50}}(\hat{p}'_T, \hat{p}_{L_2})$	0.0129771	$\ \Gamma_{\hat{p}'_T \rightarrow \hat{p}_{L_2}}(\hat{v}'_T) - \hat{v}_{L_2}\ $	0.0008360

These results are displayed in Figure 3 and Table 4. In Figure 3, each of the six geodesics are visualized as a sequence of ten shapes,  $\text{Exp}(\hat{p}, (t - \bar{x})\hat{v})$ , where  $t = 50, 55, \dots, 90, 95$ ,  $\bar{x}$  is the mean age 74.75, and  $(\hat{p}, \hat{v})$  is the regression estimate. Most of the figures look similar to Figure 3a, while Figure 3d is highly distorted. Table 4 provides a more precise comparison through the actual parameter estimates. The first two rows show that the two robust estimators perform reasonably well on the untampered dataset, though the  $L_1$  estimator performs significantly better. We observe in the last two rows that the reverse is true, to a much lesser extent, on the tampered dataset. The  $L_2$  estimator, on the other hand, performs almost an order

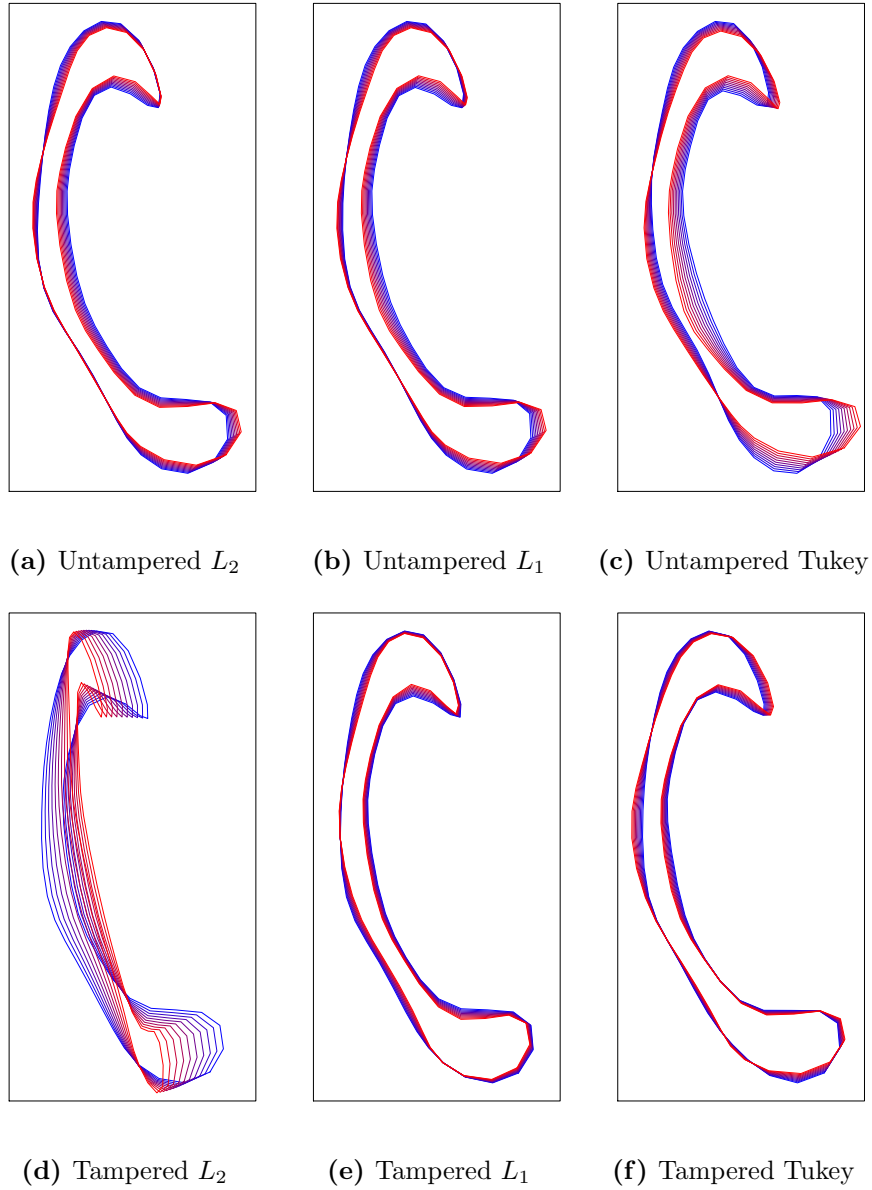


**Figure 3:** The resulting geodesics displayed as a sequence of shapes. Each subfigure contains ten shapes, representing the estimated shape at every five years from age 50 (blue) to age 95 (red).

of magnitude worse than either robust estimator on the tampered data, as seen in the third row. All of these observations fall in line with our expectations about the three estimators on data with and without outliers in a very high-dimensional compact manifold; namely, that the  $L_1$  and Tukey biweight estimators would be much more robust than the  $L_2$  estimator, and that the  $L_1$  estimator would fare better than the Tukey biweight estimator on data without

outliers.

## 5 Conclusion

In this paper, we have proposed robust estimators for geodesic regression that are resistant to outliers. These methods adapted M-type estimators, including the  $L_1$ , Huber and Tukey biweight estimators, to a manifold setting. For the M-type estimators, we have developed a method, using tangent space approximations, for calculating the tuning parameters that ensures efficiency in the case of Gaussian errors while providing protection against outliers. We have also provided justification for the preferential use of the  $L_1$  estimator over the  $L_2$  and Huber estimators on high-dimensional manifolds. Finally, the proposed methods have been evaluated on synthetic and real data.

A potentially fruitful avenue for future research is asymmetric loss functions on Riemannian manifolds. For example, quantile regression would require developing the notion of quantiles for manifold-valued data. One could also explore pseudo-quantiles, such as expectiles and M-quantiles, on manifolds.

## 6 Proofs and Derivations

### 6.1 Proof of Proposition 1

*Proof.* We first note that the term in (10) is finite because  $\rho(t) > \rho(0)$  for all  $t \in \mathbb{R}$ , which means that

$$C(\mu, b, \rho) \leq \int_M \exp\left(-\frac{\rho(0)}{b}\right) dy = \exp\left(-\frac{\rho(0)}{b}\right) \text{Vol}(M) < \infty,$$

where  $\text{Vol}(M)$  is the volume of  $M$ ;  $\text{Vol}(M)$  is finite because the diameter of  $M$  is finite. So the function in (9) is a well-defined density function.

The log-likelihood of the observations  $\{(x_i, y_i)\}_{1, \dots, N}$  under the distribution in (9) is

$$\sum_{i=1}^N \log\{C(\text{Exp}(p, Vx_i), b, \rho)\} - \frac{1}{b} \sum_{i=1}^N \rho(d(\text{Exp}(p, Vx_i), y_i)). \quad (17)$$

Because  $M$  is a symmetric space, it is also a homogeneous space, meaning that for any two points on the manifold, there exists an isometry which maps one to the other. Because the integral in (10) depends only on the distance from  $\mu$  to  $y$ , it is invariant to isometries, so the expression is independent of  $\mu$ . Therefore the first sum in (17) is constant with respect to  $p$  and  $V$ . Comparing the second sum to (8), we find that the parameters  $(p, V) \in M \times T_p M^n$  that minimize  $L_\rho(p, V)$  also maximize the log-likelihood.  $\square$

## 6.2 Derivations for cutoff parameters and efficiency of the $L_1$ estimator

This section expands upon Section 3.2, using the same notation and approximations. We make use of the beta function  $B(x, y)$ , the gamma function  $\Gamma(a)$ , the lower incomplete gamma function  $\gamma(a, z)$ , the upper incomplete gamma function  $\Gamma(a, z)$ , the lower and upper regularized gamma function  $P(a, z) = \gamma(a, z)/\Gamma(z)$  and  $Q(a, z) = \Gamma(a, z)/\Gamma(a)$ , respectively, and the inverses of the two regularized gamma functions  $P^{-1}(a, z)$  and  $Q^{-1}(a, z)$ . We also require partial derivatives of the upper and lower incomplete gamma functions:  $\frac{\partial}{\partial a}\Gamma(a, z) = -a^{z-1}e^{-a}$  and  $\frac{\partial}{\partial a}\gamma(a, z) = -\frac{\partial}{\partial a}\Gamma(a, z) = a^{z-1}e^{-a}$ , respectively. We assume  $k \geq 2$ . However, as mentioned in Section 3.2, the formulae for  $\xi$  and the approximate AREs for the Tukey biweight and  $L_1$  estimators, including their derivatives, turn out to still be valid in the  $k = 1$  case, and similarly for the Huber estimator if the second summands in (27), (31), and (33) are set to zero. The main problem when  $k = 1$  in these summands is that the upper gamma function  $\Gamma(a, z)$  is undefined when  $a = 0$ .

### 6.2.1 Identities

Before proceeding, four identities related to integrals are derived. Recall that the density of a standard  $k$ -variate Gaussian random variable is defined as  $\phi_k = (2\pi)^{-\frac{k}{2}} \exp(-\sum_{j=1}^k (y^j)^2)$ . Using the spherical coordinate system,  $r^2 = \sum_{j=1}^k (y^j)^2$ ,  $y^1 = r \sin(\theta_1) \cdots \sin(\theta_{k-2}) \sin(\theta_{k-1})$  and  $y^j = r \sin(\theta_1) \cdots \sin(\theta_{k-j}) \cos(\theta_{k-j+1})$  for  $j = 2, \dots, k$ , so that  $dy = dy_1 \cdots dy_k =$

$r^{k-1}\sin^{k-2}(\theta_1)\cdots\sin(\theta_{k-2})d\theta_{k-1}\cdots d\theta_1$ . Take a function  $g : \mathbb{R}^+ \rightarrow \mathbb{R}$ . Letting  $B_R \subset \mathbb{R}^k$  denote the  $k$ -ball centered at 0 of radius  $R$ , it follows that

$$\begin{aligned}
& \int_{B_R} g(r)\phi_k(y)dy \\
&= \int_0^R \int_0^\pi \cdots \int_0^\pi \int_0^{2\pi} g(r) \frac{1}{(2\pi)^{\frac{k}{2}}} e^{-r^2} r^{k-1} \sin^{k-2}(\theta_1) \cdots \sin(\theta_{k-2}) d\theta_{k-1} \cdots d\theta_1 dr \\
&= \frac{1}{(2\pi)^{\frac{k}{2}}} \left( \int_0^R g(r) r^{k-1} e^{-r^2} dr \right) \left( \int_0^\pi \sin^{k-2}(\theta_1) d\theta_1 \right) \cdots \\
&\quad \cdots \left( \int_0^\pi \sin^2(\theta_{k-3}) d\theta_{k-3} \right) \left( \int_0^\pi \sin(\theta_{k-2}) d\theta_{k-2} \right) \left( \int_0^{2\pi} d\theta_{k-1} \right) \\
&= \frac{1}{(2\pi)^{\frac{k}{2}}} \left( \int_0^R g(r) r^{k-1} e^{-r^2} dr \right) \left( 2 \int_0^{\pi/2} \sin^{k-2}(\theta_1) d\theta_1 \right) \cdots \\
&\quad \cdots \left( 2 \int_0^{\pi/2} \sin^2(\theta_{k-3}) d\theta_{k-3} \right) \left( 2 \int_0^{\pi/2} \sin(\theta_{k-2}) d\theta_{k-2} \right) \left( 4 \int_0^{\pi/2} d\theta_{k-1} \right) \\
&= \frac{1}{(2\pi)^{\frac{k}{2}}} \left( \int_0^R g(r) r^{k-1} e^{-r^2} dr \right) B\left(\frac{k-1}{2}, \frac{1}{2}\right) \cdots B\left(\frac{2}{2}, \frac{1}{2}\right) \cdot 2B\left(\frac{1}{2}, \frac{1}{2}\right) \\
&= \frac{1}{(2\pi)^{\frac{k}{2}}} \left( \int_0^R g(r) r^{k-1} e^{-r^2} dr \right) \frac{\Gamma(\frac{k-1}{2})\Gamma(\frac{1}{2})}{\Gamma(\frac{k}{2})} \cdots \frac{\Gamma(\frac{2}{2})\Gamma(\frac{1}{2})}{\Gamma(\frac{3}{2})} \cdot 2 \frac{\Gamma(\frac{1}{2})\Gamma(\frac{1}{2})}{\Gamma(\frac{2}{2})} \\
&= \frac{1}{(2\pi)^{\frac{k}{2}}} \left( \int_0^R g(r) r^{k-1} e^{-r^2} dr \right) \frac{2\pi^{\frac{k}{2}}}{\Gamma(\frac{k}{2})} \\
&= 2^{-\frac{k}{2}} \frac{2}{\Gamma(\frac{k}{2})} \left( \int_0^R g(r) r^{k-1} e^{-r^2} dr \right) \\
&= 2^{-\frac{k}{2}} \cdot \frac{k}{\Gamma(\frac{k+2}{2})} \left( \int_0^R g(r) r^{k-1} e^{-r^2} dr \right), \tag{18}
\end{aligned}$$

where  $\Gamma(1/2) = \pi^{1/2}$ ,  $\Gamma(1) = 1$  and  $\Gamma(z+1) = z\Gamma(z)$ . The next two identities are derived in similar fashion:

$$\begin{aligned}
& \int_{B_R} g(r)(y^1)^2 \phi_k(y) dy \\
&= \int_0^R \int_0^\pi \cdots \int_0^\pi \int_0^{2\pi} g(r) (r \sin(\theta_1) \cdots \sin(\theta_{k-2}) \sin(\theta_{k-1}))^2 \frac{1}{(2\pi)^{\frac{k}{2}}} e^{-r^2} r^{k-1} \\
&\quad \sin^{k-2}(\theta_1) \cdots \sin(\theta_{k-2}) d\theta_{k-1} \cdots d\theta_1 dr \\
&= \int_0^R \int_0^\pi \cdots \int_0^\pi \int_0^{2\pi} g(r) \frac{1}{(2\pi)^{\frac{k}{2}}} e^{-r^2} r^{k+1} \sin^k(\theta_1) \cdots \sin^2(\theta_{k-1}) d\theta_{k-1} \cdots d\theta_1 dr
\end{aligned}$$

$$\begin{aligned}
&= \frac{1}{(2\pi)^{\frac{k}{2}}} \left( \int_0^R g(r) r^{k+1} e^{-r^2} dr \right) \frac{\Gamma(\frac{k+1}{2})\Gamma(\frac{1}{2})}{\Gamma(\frac{k+2}{2})} \dots \frac{\Gamma(\frac{4}{2})\Gamma(\frac{1}{2})}{\Gamma(\frac{5}{2})} \cdot 2 \frac{\Gamma(\frac{3}{2})\Gamma(\frac{1}{2})}{\Gamma(\frac{4}{2})} \\
&= 2^{-\frac{k}{2}} \cdot \frac{1}{\Gamma(\frac{k+2}{2})} \left( \int_0^R g(r) r^{k+1} e^{-r^2} dr \right)
\end{aligned} \tag{19}$$

and

$$\begin{aligned}
&\int_{B_R} g(r) y^1 y^2 \phi_k(y) dy \\
&= \int_0^R \int_0^\pi \dots \int_0^\pi \int_0^{2\pi} g(r) (r \sin(\theta_1) \dots \sin(\theta_{k-2}) \sin(\theta_{k-1})) (r \sin(\theta_1) \dots \sin(\theta_{k-2}) \cos(\theta_{k-1})) \\
&\quad \frac{1}{(2\pi)^{\frac{k}{2}}} e^{-r^2} r^{k-1} \sin^{k-2}(\theta_1) \dots \sin(\theta_{k-2}) d\theta_{k-1} \dots d\theta_1 dr \\
&= \frac{1}{(2\pi)^{\frac{k}{2}}} \left( \int_0^R g(r) r^{k-1} e^{-r^2} dr \right) \left( \int_0^\pi \sin^k(\theta_1) d\theta_1 \right) \dots \\
&\quad \dots \left( \int_0^\pi \sin^3(\theta_{k-2}) d\theta_{k-2} \right) \left( \int_0^{2\pi} \sin(\theta_{k-1}) \cos(\theta_{k-1}) d\theta_{k-1} \right) \\
&= 0,
\end{aligned} \tag{20}$$

because  $\sin(\theta_{k-1})\cos(\theta_{k-1}) = \sin(2\theta_{k-1})/2$ , so the last factor is zero. The final identity uses the substitution  $r' = r^2/2$  and  $dr = [(r')^{-\frac{1}{2}}/\sqrt{2}]dr'$ ,

$$\begin{aligned}
\int_0^R r^m e^{-r^2} dr &= \int_0^{\frac{R^2}{2}} 2^{\frac{m-1}{2}} (r')^{\frac{m-1}{2}} e^{-r'} dr' \\
&= 2^{\frac{m-1}{2}} \cdot \gamma\left(\frac{m+1}{2}, \frac{R^2}{2}\right) \\
&= 2^{\frac{m-1}{2}} \cdot \left[ \Gamma\left(\frac{m+1}{2}\right) - \Gamma\left(\frac{m+1}{2}, \frac{R^2}{2}\right) \right].
\end{aligned} \tag{21}$$

### 6.2.2 Detailed Steps

The first step uses  $MAD = \text{Median}(\|e_1\|, \dots, \|e_N\|)$  to find a robust estimate of  $\sigma$  in (11). In the manifold case,  $e_i = \text{Log}(\text{Exp}(p, x_i v), y_i)$ . For a random variable  $Y^*$  distributed according to  $f(y) = \phi_k(y)$ , the goal is to find a factor  $\xi$  such that  $\Pr(\|Y^*\| < \xi) = 1/2$ . Letting  $g(r) = 1$

in (18) and  $m = k - 1$  in (21), we have

$$\begin{aligned}
\Pr(\|Y^*\| < \xi) &= \int_{B_\xi} \phi_k(y) dy = 2^{-\frac{k}{2}} \frac{k}{\Gamma(\frac{k+2}{2})} \left( \int_0^\xi r^{k-1} e^{-r^2} dr \right) \\
&= 2^{-\frac{k}{2}} \frac{k}{\Gamma(\frac{k+2}{2})} \cdot 2^{\frac{k-2}{2}} \cdot \gamma\left(\frac{k}{2}, \frac{\xi^2}{2}\right) \\
&= 2^{-1} \frac{2}{\Gamma(\frac{k}{2})} \cdot \gamma\left(\frac{k}{2}, \frac{\xi^2}{2}\right) \\
&= P\left(\frac{k}{2}, \frac{\xi^2}{2}\right) = \frac{1}{2}.
\end{aligned}$$

The solution to this equation is given by (12). Finally, we obtain  $\hat{\sigma} = MAD/\xi$ .

The next step finds the multiple of  $\sigma$  that gives an ARE to the sample mean of 95%, assuming a Gaussian distribution. It requires the four identities (18), (19), (20) and (21). We take a manifold-valued random variable  $W \in M$  with intrinsic mean  $\mu_W$ . If  $W^* := \text{Log}(\mu_W, W)$  has an isotropic Gaussian distribution in  $\mathbb{R}^k$  i.e. its covariance  $\Sigma_W = \sigma_W^2 I_k$  is a multiple of the identity matrix, then

$$\frac{1}{\sigma_W^2} \mathbb{E}(\|\text{Log}(\mu_W, W)\|^2) = \mathbb{E}((W^*)^T \Sigma_W^{-1} W^*) = k \implies \text{Var}(W) = k\sigma_W^2. \quad (22)$$

as  $(W^*)^T \Sigma_W^{-1} W^* \sim \chi^2(k)$ ; here we have used the definition of the variance of a manifold-valued random variable in (4). Recall that  $Y_i$ ,  $i = 1, \dots, n$ , are distributed to (11) and  $Y_i^* := \text{Log}(\mu, \hat{Y})$ . Let  $\bar{Y}$  be the sample intrinsic mean of  $Y_i$  and  $\hat{Y}$  be a sample M-type estimator. Then we define  $\bar{Y}^* = \text{Log}(\mu, \bar{Y})$  and  $\hat{Y}^* = \text{Log}(\mu, \hat{Y})$ . Assuming the latter two converge in distribution to  $N(0, \sigma_1^2 I_k)$  and  $N(0, \sigma_2^2 I_k)$ , respectively,

$$\text{ARE}(\hat{Y}, \bar{Y}) \approx \frac{k\sigma_1^2}{k\sigma_2^2} = \frac{\sigma_1^2}{\sigma_2^2} \quad (23)$$

by (4) and (22), so we just need to find  $\sigma_1^2$  and  $\sigma_2^2$ .

The covariance matrix of a sample M-type estimator can be obtained using its related influence function. For a loss function  $\rho : \mathbb{R} \rightarrow \mathbb{R}$ , define  $\|\rho\| : \mathbb{R}^k \rightarrow \mathbb{R}$  by  $\|\rho\|(t) = \rho(\|y\|)$ . Then define  $\psi : \mathbb{R}^k \rightarrow \mathbb{R}^k$  by  $\psi(y) = \nabla_y \|\rho\|(e)$ . Note that this coincides with the definition of  $\psi$  as  $\rho'$  in the  $k = 1$  case. If  $F$  is the distribution of  $e$ , and  $T(F)$ , the statistical functional at

$F$  representing the M-type estimator, is the solution to  $\mathbb{E}_F[\psi(y - T(F))]$ , then the influence function at  $y_0 \in \mathbb{R}^k$  is defined as

$$IF(y_0; T, F) = \mathbb{E}(J_\psi(y - T(F)))^{-1} \psi(y_0 - T(F)),$$

where  $J_\psi$  denotes the Jacobian matrix of  $\psi$ . It is known by the central limit theorem that for the sample M-type estimator,  $T(\hat{F})$ , it follows that

$$\sqrt{N}(T(\hat{F}) - T(F)) \Rightarrow N\left(0, \int IF(y; T, F)IF(y; T, F)^T dF(y)\right).$$

Since  $T(F) = \mu = 0$  in our case, the covariance of the sample M-type estimator is asymptotically given by

$$\Sigma_\psi = \frac{1}{N} (\mathbb{E}(J_\psi(y))^{-1})^2 \mathbb{E}[\psi(y)\psi(y)^T]. \quad (24)$$

The covariance of the sample mean  $\bar{Y}^* = (1/N) \sum_{i=1}^N Y_i^*$  is simply

$$\frac{1}{N} \text{Cov}(Y_1^*) = \frac{1}{N} I_k, \quad (25)$$

so  $\sigma_1^2 = 1/N$  in (23).

(a) **Huber estimator:** In the case of the Huber estimator, we have

$$\psi_H(y) = \begin{cases} y & \text{if } \|y\| < c \\ c \cdot \frac{y}{\|y\|} & \text{otherwise,} \end{cases} \quad \text{and} \quad J_{\psi_H}(y) = \begin{cases} I_k & \text{if } \|y\| < c \\ c \left( \frac{1}{\|y\|} I_k - \frac{1}{\|y\|^3} y y^T \right) & \text{otherwise.} \end{cases} \quad (26)$$

We first consider the first matrix term in (24). Using the identity of (20),  $\mathbb{E}(J_{\psi_H}(y))_{12} = -\int_{B_c^c} \frac{1}{\|y\|^3} (y^1)(y^2) \phi_k(y) dy = 0$ . On the other hand, using the identities (18), (19), and (21),

$$\begin{aligned} \mathbb{E}(J_{\psi_H}(y))_{11} &= \int_{B_c} \phi_k(y) dy + c \int_{B_c^c} \frac{1}{\|y\|} \phi_k(y) dy - c \int_{B_c^c} \frac{1}{\|y\|^3} (y^1)^2 \phi_k(y) dy \\ &= 2^{-\frac{k}{2}} \cdot \frac{k}{\Gamma(\frac{k+2}{2})} \left( \int_0^c r^{k-1} e^{-r^2} dr \right) + c \cdot 2^{-\frac{k}{2}} \cdot \frac{k}{\Gamma(\frac{k+2}{2})} \left( \int_c^\infty \frac{1}{r} r^{k-1} e^{-r^2} dr \right) \\ &\quad - c \cdot 2^{-\frac{k}{2}} \cdot \frac{1}{\Gamma(\frac{k+2}{2})} \left( \int_c^\infty \frac{1}{r^3} r^{k-1} e^{-r^2} dr \right) \end{aligned}$$

$$\begin{aligned}
&= \frac{1}{\Gamma\left(\frac{k+2}{2}\right)} \left\{ 2^{-\frac{k}{2}} \cdot k \cdot 2^{\frac{k-2}{2}} \cdot \gamma\left(\frac{k}{2}, \frac{c^2}{2}\right) + c \cdot 2^{-\frac{k}{2}} \cdot k \cdot 2^{\frac{k-3}{2}} \cdot \left[\Gamma\left(\frac{k-1}{2}\right) \right. \right. \\
&\quad \left. \left. - \gamma\left(\frac{k-1}{2}, \frac{c^2}{2}\right)\right] - c \cdot 2^{-\frac{k}{2}} \cdot 2^{\frac{k-3}{2}} \cdot \left[\Gamma\left(\frac{k-1}{2}\right) - \gamma\left(\frac{k-1}{2}, \frac{c^2}{2}\right)\right] \right\} \\
&= \frac{1}{\Gamma\left(\frac{k+2}{2}\right)} \left\{ \frac{k}{2} \gamma\left(\frac{k}{2}, \frac{c^2}{2}\right) + 2^{-\frac{3}{2}} c (k-1) \Gamma\left(\frac{k-1}{2}, \frac{c^2}{2}\right) \right\}. \tag{27}
\end{aligned}$$

By symmetry,  $E(J_{\psi_H}(y))_{jj} = E(J_{\psi_H}(y))_{11}$  for  $j = 1, \dots, k$ , and  $E(J_{\psi_H}(y))_{lj} = E(J_{\psi_H}(y))_{12}$  for all  $j, l = 1, \dots, k$ ,  $l \neq j$ , so the covariance of the sample mean is a scalar multiple of the identity matrix; namely,  $E(J_{\psi_H}(y))$  is  $I_k$  multiplied by the result of (27).

We now consider the second matrix term in (24). The non-diagonal terms can again be shown to be zero using identity (20) and symmetry, and the diagonal terms can be shown to be equal by symmetry. Then with  $\psi_H = (\psi_H^1, \dots, \psi_H^k)$  in (26), it follows that

$$\begin{aligned}
E[\psi_H(y)\psi_H(y)^T]_{11} &= E[(\psi_H^1(y))^2] \\
&= \int_{B_c} (y^1)^2 \phi_k(y) dy + c^2 \int_{B_c^c} \frac{1}{\|y\|^2} (y^1)^2 \phi_k(y) dy \\
&= \frac{2^{-\frac{k}{2}}}{\Gamma\left(\frac{k+2}{2}\right)} \left( \int_0^c r^{k+1} e^{-r^2} dr \right) + c^2 \cdot \frac{2^{-\frac{k}{2}}}{\Gamma\left(\frac{k+2}{2}\right)} \left( \int_c^\infty r^{k-1} e^{-r^2} dr \right) \\
&= \frac{1}{\Gamma\left(\frac{k+2}{2}\right)} \left\{ \gamma\left(\frac{k+2}{2}, \frac{c^2}{2}\right) + \frac{c^2}{2} \Gamma\left(\frac{k}{2}, \frac{c^2}{2}\right) \right\}, \tag{28}
\end{aligned}$$

again using (19) and (21). Thus, the matrix  $E[\psi_H(y)\psi_H(y)^T]$  is the above expression multiplied by  $I_k$ , and the variance  $\Sigma_\psi$  in (24) can be calculated using (27) and (28),

$$\Sigma_{\psi_H} = \frac{E[\psi_H(y)\psi_H(y)^T]_{11}}{N(E(J_{\psi_H}(y))_{11})^2} \cdot I_k, \tag{29}$$

giving our  $\sigma_2^2$  in (23). Hence, from (23), (25), (27), (28), and (29), the approximate ARE to the sample mean is given by (13)

$$\text{ARE}_{H,L_2}(c, k) \approx A_H(c, k) := \frac{H_1^2}{\Gamma\left(\frac{k+2}{2}\right) H_2}, \tag{30}$$

where

$$H_1 = \Gamma\left(\frac{k+2}{2}\right)\mathbb{E}(J_{\psi_H}(y))_{11} = \frac{k}{2}\gamma\left(\frac{k}{2}, \frac{c^2}{2}\right) + 2^{-\frac{3}{2}}c(k-1)\Gamma\left(\frac{k-1}{2}, \frac{c^2}{2}\right), \quad (31)$$

$$H_2 = \Gamma\left(\frac{k+2}{2}\right)\mathbb{E}[\psi_H(y)\psi_H(y)^T]_{11} = \gamma\left(\frac{k+2}{2}, \frac{c^2}{2}\right) + \frac{c^2}{2}\Gamma\left(\frac{k}{2}, \frac{c^2}{2}\right). \quad (32)$$

Lastly, we apply the Newton-Raphson method to find the value of  $c$  for which the ARE is approximately 95%, that is, the solution in  $c$  to the equation  $A_H(c, k) - 0.95 = 0$ . This requires the partial derivative of  $A_H(c, k)$  with respect to  $c$ ,

$$\frac{\partial}{\partial c}A_H(c, k) = \frac{2H_1H_3H_2 - H_1^2H_4}{\Gamma\left(\frac{k+2}{2}\right)H_2^2},$$

where  $H_1$  and  $H_2$  are as above and

$$\begin{aligned} H_3 &= \frac{\partial}{\partial c}H_1 \\ &= \frac{ck}{2}\left(\frac{c^2}{2}\right)^{\frac{k-2}{2}}e^{-\frac{c^2}{2}} + 2^{-\frac{3}{2}}(k-1)\Gamma\left(\frac{k-1}{2}, \frac{c^2}{2}\right) - 2^{-\frac{3}{2}}c^2(k-1)\left(\frac{c^2}{2}\right)^{\frac{k-3}{2}}e^{-\frac{c^2}{2}} \\ &= 2^{-\frac{k}{2}}c^{k-1}e^{-\frac{c^2}{2}} + 2^{-\frac{3}{2}}(k-1)\Gamma\left(\frac{k-1}{2}, \frac{c^2}{2}\right), \end{aligned} \quad (33)$$

$$\begin{aligned} H_4 &= \frac{\partial}{\partial c}H_2 \\ &= c\left(\frac{c^2}{2}\right)^{\frac{k}{2}}e^{-\frac{c^2}{2}} + c\Gamma\left(\frac{k}{2}, \frac{c^2}{2}\right) - c\left(\frac{c^2}{2}\right)\left(\frac{c^2}{2}\right)^{\frac{k-2}{2}}e^{-\frac{c^2}{2}} \\ &= c\Gamma\left(\frac{k}{2}, \frac{c^2}{2}\right). \end{aligned} \quad (34)$$

(b) **Tukey biweight estimator:** For this estimator, it is easy to show that

$$\psi_B(y) = \begin{cases} \left[1 - \left(\frac{\|y\|}{c}\right)^2\right]^2 \cdot y & \text{if } \|y\| < c \\ 0 & \text{otherwise,} \end{cases}$$

and

$$J_{\psi_B}(y) = \begin{cases} \left[1 - \left(\frac{\|y\|}{c}\right)^2\right]^2 I_k - \frac{4}{c^2} \left[1 - \left(\frac{\|y\|}{c}\right)^2\right] yy^T & \text{if } \|y\| < c \\ 0 & \text{otherwise.} \end{cases}$$

By similar arguments to the ones used for the Huber estimator, we have  $E(J_{\psi_B}(y))_{12} = 0$ ,  $E[\psi_H(y)\psi_H(y)^T]_{12} = 0$ ,

$$E(J_{\psi_H}(y))_{11} = \frac{1}{\Gamma(\frac{k+2}{2})} \left\{ \frac{2(k+4)}{c^4} \gamma\left(\frac{k+4}{2}, \frac{c^2}{2}\right) - \frac{2(k+2)}{c^2} \gamma\left(\frac{k+2}{2}, \frac{c^2}{2}\right) + \frac{k}{2} \gamma\left(\frac{k}{2}, \frac{c^2}{2}\right) \right\}, \quad (35)$$

$$E[\psi_H(y)\psi_H(y)^T]_{11} = \frac{1}{\Gamma(\frac{k+2}{2})} \left\{ \gamma\left(\frac{k+2}{2}, \frac{c^2}{2}\right) - \frac{8}{c^2} \gamma\left(\frac{k+4}{2}, \frac{c^2}{2}\right) + \frac{24}{c^4} \gamma\left(\frac{k+6}{2}, \frac{c^2}{2}\right) - \frac{32}{c^6} \gamma\left(\frac{k+8}{2}, \frac{c^2}{2}\right) + \frac{16}{c^8} \gamma\left(\frac{k+10}{2}, \frac{c^2}{2}\right) \right\}. \quad (36)$$

Thus, the variance  $\Sigma_\psi$  in (24) can be calculated using (35) and (36),

$$\Sigma_{\psi_B} = \frac{E[\psi_B(y)\psi_B(y)^T]_{11}}{N(E(J_{\psi_B}(y))_{11})^2} \cdot I_k. \quad (37)$$

giving our  $\sigma_2^2$  in (23). Therefore, from (23), (25), (35), (36), and (37), the approximate ARE to the sample mean is given by (14),

$$\text{ARE}_{T,L_2}(c, k) \approx A_T(c, k) := \frac{T_1^2}{\Gamma(\frac{k+2}{2})T_2},$$

where

$$\begin{aligned} T_1 &= \Gamma\left(\frac{k+2}{2}\right) E(J_{\psi_T}(y))_{11} = \frac{2(k+4)}{c^4} \gamma\left(\frac{k+4}{2}, \frac{c^2}{2}\right) - \frac{2(k+2)}{c^2} \gamma\left(\frac{k+2}{2}, \frac{c^2}{2}\right) + \frac{k}{2} \gamma\left(\frac{k}{2}, \frac{c^2}{2}\right), \\ T_2 &= \Gamma\left(\frac{k+2}{2}\right) E[\psi_T(y)\psi_H(y)^T]_{11} = \gamma\left(\frac{k+2}{2}, \frac{c^2}{2}\right) - \frac{8}{c^2} \gamma\left(\frac{k+4}{2}, \frac{c^2}{2}\right) + \frac{24}{c^4} \gamma\left(\frac{k+6}{2}, \frac{c^2}{2}\right) \\ &\quad - \frac{32}{c^6} \gamma\left(\frac{k+8}{2}, \frac{c^2}{2}\right) + \frac{16}{c^8} \gamma\left(\frac{k+10}{2}, \frac{c^2}{2}\right). \end{aligned}$$

We solve for the root of the function  $A_T(c, k) - 0.95$  by utilizing  $\frac{\partial}{\partial c} A_T(c, k)$  in the Newton-Raphson method,

$$\frac{\partial}{\partial c} A_T(c, k) = \frac{2T_1 T_3 T_2 - T_1^2 T_4}{\Gamma(\frac{k+2}{2}) T_2^2},$$

where  $T_1$  and  $T_2$  are as above and

$$\begin{aligned}
T_3 &= \frac{\partial}{\partial c} T_1 \\
&= -\frac{8(k+4)}{c^5} \gamma\left(\frac{k+4}{2}, \frac{c^2}{2}\right) + \frac{2(k+2)}{c^3} \left(\frac{c^2}{2}\right)^{\frac{k+2}{2}} e^{-\frac{c^2}{2}} + \frac{4(k+2)}{c^3} \gamma\left(\frac{k+2}{2}, \frac{c^2}{2}\right) \\
&\quad - \frac{2(k+2)}{c} \left(\frac{c^2}{2}\right)^{\frac{k}{2}} e^{-\frac{c^2}{2}} + \frac{ck}{2} \left(\frac{c^2}{2}\right)^{\frac{k-2}{2}} e^{-\frac{c^2}{2}} \\
&= -\frac{8(k+4)}{c^5} \gamma\left(\frac{k+4}{2}, \frac{c^2}{2}\right) + \frac{4(k+2)}{c^3} \gamma\left(\frac{k+2}{2}, \frac{c^2}{2}\right) - 2^{-\frac{k-2}{2}} c^{k-1} e^{-\frac{c^2}{2}}, \\
T_4 &= \frac{\partial}{\partial c} T_2 \\
&= c \left(\frac{c^2}{2}\right)^{\frac{k}{2}} e^{-\frac{c^2}{2}} + \frac{16}{c^3} \gamma\left(\frac{k+4}{2}, \frac{c^2}{2}\right) - \frac{8}{c} \left(\frac{c^2}{2}\right)^{\frac{k+2}{2}} e^{-\frac{c^2}{2}} - \frac{96}{c^5} \gamma\left(\frac{k+6}{2}, \frac{c^2}{2}\right) + \frac{24}{c^3} \left(\frac{c^2}{2}\right)^{\frac{k+4}{2}} e^{-\frac{c^2}{2}} \\
&\quad + \frac{192}{c^7} \gamma\left(\frac{k+8}{2}, \frac{c^2}{2}\right) - \frac{32}{c^5} \left(\frac{c^2}{2}\right)^{\frac{k+6}{2}} e^{-\frac{c^2}{2}} - \frac{128}{c^9} \gamma\left(\frac{k+10}{2}, \frac{c^2}{2}\right) + \frac{16}{c^7} \left(\frac{c^2}{2}\right)^{\frac{k+8}{2}} e^{-\frac{c^2}{2}} \\
&= \frac{16}{c^3} \gamma\left(\frac{k+4}{2}, \frac{c^2}{2}\right) - \frac{96}{c^5} \gamma\left(\frac{k+6}{2}, \frac{c^2}{2}\right) + \frac{192}{c^7} \gamma\left(\frac{k+8}{2}, \frac{c^2}{2}\right) - \frac{128}{c^9} \gamma\left(\frac{k+10}{2}, \frac{c^2}{2}\right).
\end{aligned}$$

### 6.3 Proof of Proposition 2

*Proof of Proposition 2(a).* Using (30), (31), (32), (33), and (34), and two applications of L'Hôpital's rule, we obtain

$$\begin{aligned}
\lim_{c \rightarrow 0} A_H(c, k) &= \lim_{c \rightarrow 0} \frac{H_1^2}{\Gamma\left(\frac{k+2}{2}\right) H_2} = \lim_{c \rightarrow 0} \frac{2H_1 H_3}{\Gamma\left(\frac{k+2}{2}\right) H_4} = \lim_{c \rightarrow 0} \frac{2H_3^2 + 2H_1 \frac{\partial}{\partial c} H_3}{\Gamma\left(\frac{k+2}{2}\right) \frac{\partial}{\partial c} H_4} \\
&= \lim_{c \rightarrow 0} \frac{2 \left\{ 2^{-\frac{k}{2}} c^{k-1} e^{-\frac{c^2}{2}} + 2^{-\frac{3}{2}} (k-1) \Gamma\left(\frac{k-1}{2}, \frac{c^2}{2}\right) \right\}^2 - 2H_1 2^{-\frac{k}{2}} c^k e^{-\frac{c^2}{2}}}{\Gamma\left(\frac{k+2}{2}\right) \left\{ \Gamma\left(\frac{k}{2}, \frac{c^2}{2}\right) - 2^{-\frac{k-2}{2}} c^{k-1} e^{-\frac{c^2}{2}} \right\}} \\
&= \frac{2 \left\{ 2^{-\frac{3}{2}} (k-1) \Gamma\left(\frac{k-1}{2}\right) \right\}^2}{\Gamma\left(\frac{k+2}{2}\right) \Gamma\left(\frac{k}{2}\right)} = \frac{\left(\frac{k-1}{2}\right)^2 \Gamma^2\left(\frac{k-1}{2}\right)}{\Gamma\left(\frac{k}{2}\right) \Gamma\left(\frac{k+2}{2}\right)} = \frac{\Gamma^2\left(\frac{k+1}{2}\right)}{\Gamma\left(\frac{k}{2}\right) \Gamma\left(\frac{k+2}{2}\right)}. \quad \square
\end{aligned}$$

**Lemma 1.** *It follows that*

$$\frac{\Gamma^2\left(\frac{k+1}{2}\right)}{\Gamma\left(\frac{k}{2}\right) \Gamma\left(\frac{k+2}{2}\right)} < \sqrt{\frac{k}{k+1}}.$$

*Proof.* Theorem 3 in Mortici (2012) states that, for  $x \geq 1$ ,

$$\frac{1}{\sqrt{x \left( 1 + \frac{1}{4x - \frac{1}{2} + \frac{3}{16x + \frac{5}{4x}}} \right)}} < \frac{\Gamma(x + \frac{1}{2})}{\Gamma(x + 1)} < \frac{1}{\sqrt{x \left( 1 + \frac{1}{4x - \frac{1}{2} + \frac{3}{16x}} \right)}} \quad (38)$$

Because  $x \geq 1$ , it follows that  $4x - \frac{1}{2} + \frac{3}{16x} \leq 4x - \frac{1}{2} + \frac{3}{16} = 4x - \frac{5}{16} < 4x$ , so we have

$$\frac{1}{\sqrt{x \left( 1 + \frac{1}{4x - \frac{1}{2} + \frac{3}{16x}} \right)}} < \frac{1}{\sqrt{x \left( 1 + \frac{1}{4x} \right)}} = \frac{1}{\sqrt{x + \frac{1}{4}}}. \quad (39)$$

Therefore, using (15) and letting  $x = \frac{k}{2} \geq 1$  in (38) and (39), we obtain

$$\frac{\Gamma^2(\frac{k+1}{2})}{\Gamma(\frac{k}{2})\Gamma(\frac{k+2}{2})} = \frac{\Gamma^2(\frac{k+1}{2})}{\frac{2}{k}\Gamma(\frac{k+2}{2})\Gamma(\frac{k+2}{2})} = \frac{k}{2} \left( \frac{\Gamma(\frac{k+1}{2})}{\Gamma(\frac{k+2}{2})} \right)^2 < \frac{\frac{k}{2}}{\frac{k}{2} + \frac{1}{4}} = \frac{2k}{2k+1}.$$

Now, for  $k \geq 2$ , it follows that  $4k^3 + 4k^2 < 4k^3 + 4k^2 + k$ . Thus, we have

$$\frac{2k}{2k+1} < \sqrt{\frac{k}{k+1}}.$$

It completes the proof. □

*Proof of Proposition 2(b).* By Lemma 1 and (15), we have

$$\begin{aligned} A_{L_1}(k+1) &= \frac{\Gamma^2(\frac{k+2}{2})}{\Gamma(\frac{k+1}{2})\Gamma(\frac{k+3}{2})} = \frac{\frac{k}{2}\Gamma(\frac{k}{2})\Gamma(\frac{k+2}{2})}{\Gamma(\frac{k+1}{2}) \cdot \frac{k+1}{2}\Gamma(\frac{k+1}{2})} = \frac{k}{k+1} \frac{1}{A_{L_1}(k)} \\ &> \frac{k}{k+1} \sqrt{\frac{k+1}{k}} = \sqrt{\frac{k}{k+1}} \\ &> A_{L_1}(k) \end{aligned}$$

for  $k \geq 2$ . □

*Proof of Proposition 2(c).* We again use (38). Because  $x \geq 1 > 0$ , it follows that  $4x - \frac{1}{2} +$

$\frac{3}{16x + \frac{15}{4x}} > 4x - \frac{1}{2} > 3x$ , and so we have

$$\frac{1}{\sqrt{x \left( 1 + \frac{1}{4x - \frac{1}{2} + \frac{3}{16x + \frac{15}{4x}}} \right)}} > \frac{1}{\sqrt{x \left( 1 + \frac{1}{3x} \right)}} = \frac{1}{\sqrt{x + \frac{1}{3}}}. \quad (40)$$

Combining (38), (39), and (40), we obtain

$$\frac{1}{\sqrt{x + \frac{1}{3}}} < \frac{\Gamma(x + \frac{1}{2})}{\Gamma(x + 1)} < \frac{1}{\sqrt{x + \frac{1}{4}}} \quad (41)$$

for  $x \geq 1$ . Taking the reciprocal of (41) and replacing  $x$  with  $x - \frac{1}{2}$  gives

$$\sqrt{(x - \frac{1}{2}) + \frac{1}{4}} < \frac{\Gamma((x - \frac{1}{2}) + 1)}{\Gamma((x - \frac{1}{2}) + \frac{1}{2})} < \sqrt{(x - \frac{1}{2}) + \frac{1}{3}}$$

or

$$\sqrt{x + \frac{1}{2}} < \frac{\Gamma(x + \frac{1}{2})}{\Gamma(x)} < \sqrt{x - \frac{1}{6}} \quad (42)$$

for  $x - \frac{1}{2} \geq 1$ , or  $x \geq \frac{3}{2}$ . Then multiplying (41) and (42) gives

$$\sqrt{\frac{x + \frac{1}{2}}{x + \frac{1}{3}}} < \frac{\Gamma^2(x + \frac{1}{2})}{\Gamma(x)\Gamma(x + 1)} < \sqrt{\frac{x - \frac{1}{6}}{x + \frac{1}{4}}} \quad (43)$$

for  $x \geq \frac{3}{2}$ . The limits as  $x \rightarrow \infty$  of the left- and right-hand expressions in (43) are both 1, and letting  $x = \frac{k}{2}$ , the central expression is (15), completing the proof.  $\square$

## Appendix

Much of this appendix has been written with reference to Section 3.11 of the online supplementary document of Cornea et al. (2017) and Section 5.2.1 of Fletcher (2013).

As mentioned in Section 4.2, a shape is the geometry of an object after the effects of translation, scaling and rotation have been removed. A  $K$ -configuration in the two-dimensional plane can be expressed as a  $K$ -by-2 matrix, or equivalently as a complex  $k$ -vector  $z = (z^1, \dots, z^K) \in \mathbb{C}^K$ . Translation is removed by subtracting the centroid  $\frac{1}{n} \sum_{m=1}^K z^m$  from

each element of  $z$  and scaling is removed by dividing  $z$  by its norm  $\|z\| = \sqrt{\langle z, z \rangle}$ ; recall that the standard complex inner product is given by  $\langle z_1, z_2 \rangle = \overline{z_2}^T z_1 = \sum_{m=1}^K z_1^m \overline{z_2^m}$ . In this way, we limit our consideration to  $D^K = \{z \in \mathbb{C}^K \mid \sum_{m=1}^K z^m = 0, \sum_{m=1}^K z^m \overline{z^m} = 1\}$ , which can be thought of as a unit sphere of real dimension  $2K - 3$ . This set is called the *pre-shape space*, and its elements *pre-shapes*.

As only rotation remains, pre-shapes have the same shape if they are planar rotations of each other. We define an equivalence relation on  $D^K$  such that all pre-shapes of the same shape are equivalent. Then two pre-shapes  $z_1, z_2 \in D^K$  are equivalent ( $z_1 \sim z_2$ ) if  $z_1 = z_2 e^{i\theta}$  for some angle  $\theta$ , as rotation in the complex plane is performed by multiplication by  $e^{i\theta}$ . So a shape is the equivalence class  $p = [z_p]_{\sim} = \{z' = z_p e^{i\theta} \mid \theta \in [0, 2\pi)\} \subset D^K$ , the set of all rotations of a pre-shape  $z_p$ , and is an element of the quotient space  $\Sigma_2^K = D^K/S^1$ , a Riemannian manifold of real dimension  $(2K - 4)$ . This space is equivalent to  $\mathbb{C}P^{K-2}$ , the set of complex lines through the origin in  $\mathbb{C}^{K-1}$ , as the space of centered  $K$ -configurations is equivalent to  $\mathbb{C}^{K-1}$ , and scaling and rotation together are equivalent to multiplication by a complex number  $re^{i\theta}$ .

The manifold is endowed with the complex inner product and the tangent space at  $y = [z_y]_{\sim} \in \Sigma_2^K$  is given by

$$\begin{aligned} T_y \Sigma_2^K &= \{v = (v^1, \dots, v^K) \mid \frac{1}{K} \sum_{m=1}^K v^m = 0 \text{ and } \operatorname{Re}(\langle z_y e^{i\theta}, v \rangle) = 0, \forall \theta \in [0, 2\pi)\} \\ &= \{v = (v^1, \dots, v^K) \mid \sum_{m=1}^K v^m = 0, \langle z', v \rangle = 0 \text{ for any } z' \in [z_y]_{\sim}\}, \end{aligned}$$

where  $\operatorname{Re}(\langle \cdot, \cdot \rangle)$  gives the real inner product when the complex  $k$ -vectors are instead conceptualized as real  $2k$ -vectors.

All calculations in shape space are done using representatives in pre-shape space. Given  $z_p, z_q \in D^K$ ,  $z_q^* = \operatorname{argmin}_{z'_q \in [z_q]_{\sim}} d_{D^K}(z_p, z'_q)$ , where  $d_{D^K}$  is the spherical geodesic distance on  $D^K$ , is the optimal rotational alignment of  $z_q$  to  $z_p$ . It can be shown that

$$z_q^* = z_q e^{i\theta^*}, \text{ where } e^{i\theta^*} = \frac{\langle z_p, z_q \rangle}{|\langle z_p, z_q \rangle|}, \quad (44)$$

so that  $\theta^*$  is the argument of  $\langle z_p, z_q \rangle$ ; note that this means  $\langle z_p, z_q^* \rangle = |\langle z_p, z_q \rangle|$  is real and positive. Then the geodesic distance  $d_{\Sigma_2^K}$  between  $p = [z_p]_{\sim}$  and  $q = [z_q]_{\sim}$  on  $\Sigma_2^K$  is

$$d_{\Sigma_2^K}(p, q) = \min_{z'_q \in [z_q]} d_{DK}(z_p, z'_q) = d_{DK}(z_p, z_q^*) = \cos^{-1}(\langle z_p, z_q^* \rangle) = \cos^{-1}(|\langle z_p, z_q \rangle|),$$

where  $z_q$  can be any element of  $[z_q]_{\sim}$  and the geodesic distance does not depend on the choice of the representative pre-shapes. The exponential map for  $\Sigma_2^K$  is given by

$$\text{Exp}(p, v) = \left[ \cos(\|v\|)z_p + \sin(\|v\|)\frac{v}{\|v\|} \right]_{\sim},$$

where  $p = [z_p]_{\sim} \in \Sigma_2^K$ ,  $v \in T_p\Sigma_2^K$ . This is similar to the exponential map for the  $k$ -sphere. Note that the resulting pre-shape in the square brackets is optimally aligned to the representative pre-shape  $z_p$ . The logarithmic map is given by

$$\text{Log}(p, q) = \cos^{-1}(\langle z_p, z_q^* \rangle) \frac{z_q^* - \langle z_p, z_q^* \rangle z_p}{\|z_q^* - \langle z_p, z_q^* \rangle z_p\|} = \cos^{-1}(|\langle z_p, z_q \rangle|) \frac{z_q^* - |\langle z_p, z_q \rangle| z_p}{\|z_q^* - |\langle z_p, z_q \rangle| z_p\|},$$

where  $p = [z_p]_{\sim}$  and  $q = [z_q]_{\sim}$  are in  $\Sigma_2^K$  and  $z_q^*$  is as defined in (44). Note that this depends on the choice of  $z_p$  but not  $z_q$ , and so is only valid at the at this particular representation of  $p$ . Parallel transport of  $v \in T_p\Sigma_2^K$  along the geodesic from  $p = [z_p]_{\sim}$  to  $q = [z_q]_{\sim}$  is

$$\begin{aligned} \Gamma_{p \rightarrow q}(v) &= e^{-i\theta^*} \left\{ v - \langle v, z_p \rangle z_p - \langle v, \tilde{z}_q^* \rangle \tilde{z}_q^* + \left( \langle z_q^*, z_p \rangle \langle v, z_p \rangle - \sqrt{1 - |\langle z_q^*, z_p \rangle|^2} \langle v, \tilde{z}_q^* \rangle \right) z_p \right. \\ &\quad \left. + \left( \sqrt{1 - |\langle z_q^*, z_p \rangle|^2} \langle v, z_p \rangle - \overline{\langle z_q^*, z_p \rangle} \langle v, \tilde{z}_q^* \rangle \right) \tilde{z}_q^* \right\} \\ &= \frac{\overline{\langle z_p, z_q \rangle}}{|\langle z_p, z_q \rangle|} \left\{ v - \langle v, z_p \rangle z_p - \langle v, \tilde{z}_q^* \rangle \tilde{z}_q^* + \left( |\langle z_p, z_q \rangle| \langle v, z_p \rangle \right. \right. \\ &\quad \left. \left. - \sqrt{1 - |\langle z_p, z_q \rangle|^2} \langle v, \tilde{z}_q^* \rangle \right) z_p + \left( \sqrt{1 - |\langle z_p, z_q \rangle|^2} \langle v, z_p \rangle - |\langle z_p, z_q \rangle| \langle v, \tilde{z}_q^* \rangle \right) \tilde{z}_q^* \right\}, \end{aligned}$$

where  $\tilde{z}_q^* = (z_q^* - \langle z_q^*, z_p \rangle z_p) / \sqrt{1 - \langle z_q^*, z_p \rangle^2} = (z_q^* - |\langle z_p, z_q \rangle| z_p) / \sqrt{1 - |\langle z_p, z_q \rangle|^2}$  and  $z_q^*, \theta^*$  are as defined in (44). Parallel transport uses the special unitary group. Note that this depends on the choice of both  $z_p$  and  $z_q$ , so care must be taken.

In the simple regression case, the exact gradients with respect to  $p$  and  $v$ , calculated using Jacobi fields, are

$$\begin{aligned}
\nabla_p E_\rho &= - \sum_{i=1}^N \frac{\rho'(\|e_i\|)}{\|e_i\|} d_p \text{Exp}(p, x_i v)^\dagger e_i \\
&= - \sum_{i=1}^N \frac{\rho'(\|e_i\|)}{\|e_i\|} \left( \cos(\|x_i v\|) u_i^\perp + \cos(\|2x_i v\|) w_i^\perp + u_i^\top + w_i^\top \right), \\
\nabla_v E_\rho &= - \sum_{i=1}^N x_i \frac{\rho'(\|e_i\|)}{\|e_i\|} d_v \text{Exp}(p, x_i v)^\dagger e_i \\
&= - \sum_{i=1}^N x_i \frac{\rho'(\|e_i\|)}{\|e_i\|} \left( \frac{\sin(\|x_i v\|)}{\|x_i v\|} u_i^\perp + \frac{\sin(\|2x_i v\|)}{\|2x_i v\|} w_i^\perp + u_i^\top + w_i^\top \right),
\end{aligned}$$

where  $e_i = \text{Log}(\hat{y}_i, y_i)$  and  $u_i, w_i$  are defined as follows: Define a function  $j : \mathbb{C} \rightarrow \mathbb{C}$  by  $j(v) = iv$ , where  $i = \sqrt{-1}$ , not the index. Separate  $\Gamma_{\hat{y}_i \rightarrow p}(e_i)$  into components  $u_i$  and  $w_i$  that are orthogonal and parallel to  $j(x_i v)$  respectively, where all these vectors are conceptualized as real  $2k$ -vectors rather than complex  $k$  vectors i.e.

$$w_i = \text{Re} \left( \left\langle \Gamma_{\hat{y}_i \rightarrow p}(e_i), \frac{j(x_i v)}{\|j(x_i v)\|} \right\rangle \right) \frac{j(x_i v)}{\|j(x_i v)\|}, \text{ and } u_i = \Gamma_{\hat{y}_i \rightarrow p}(e_i) - w_i.$$

Then  $u_i^\perp$  and  $u_i^\top$  are defined by

$$u_i^\top = \text{Re} \left( \left\langle u_i, \frac{v}{\|v\|} \right\rangle \right) \frac{v}{\|v\|}, \text{ and } u_i^\perp = u_i - u_i^\top,$$

again treating the complex  $k$ -vectors as real  $2k$ -vectors, and  $w_i^\perp$  and  $w_i^\top$  are defined similarly.

## Acknowledgement

This research was supported by the Basic Science Research Program through the National Research Foundation of Korea (NRF) grant, funded by the government of Korea (2018R1D1A1B07042933).

## References

- Banerjee, M., Chakraborty, R., Ofori, E., Okun, M. S., Vaillancourt, D. E. and Vemuri, B. C. (2016). A nonlinear regression technique for manifold valued data with applications to medical image analysis. *2016 IEEE Conference on Computer Vision and Pattern Recognition (CVPR)*, 4424–4432.
- Cheng, G. and Vemuri, B. C. (2013). A novel dynamic system in the space of SPD matrices with applications to appearance tracking. *SIAM Journal on Imaging Sciences*, **6**, 592–615.
- Cornea, E., Zhu, H., Kim, P. and Ibrahim, J. G. (2017). Regression models on Riemannian symmetric spaces. *Journal of the Royal Statistical Society: Series B*, **79**, 463–482.
- Davis, B. C., Fletcher, P. T., Bullitt, E. and Joshi, S. (2010). Population shape regression from random design data. *International Journal of Computer Vision*, **90**, 255–266.
- do Carmo, M. (1992). *Riemannian Geometry*. Birkhäuser, Boston.
- Du, J., Goh, A., Kushnarev, S. and Qiu, A. (2014). Geodesic regression on orientation distribution functions with its application to an aging study. *NeuroImage*, **87**, 416–426.
- Fletcher, P. T. (2013). Geodesic regression and the theory of least squares on Riemannian manifolds. *International Journal of Computer Vision*, **105**, 171–185.
- Fletcher, P. T., Lu, C., Pizer, S.M. and Joshi, S. (2004). Principal geodesic analysis for the study of nonlinear statistics of shape. *IEEE Transactions on Medical Imaging*, **23**, 995–1005.
- Fréchet, M. (1948). Les éléments aléatoires de nature quelconque dans un espace distancié. *Annales de l'Institut Henri Poincaré*, **10**, 215–310.
- Hein, M. (2009). Robust nonparametric regression with metric-space valued output. *Advances in Neural Information Processing Systems 22*.
- Hinkle, J., Fletcher, P. T. and Joshi, S. (2014). Intrinsic polynomials for regression on Riemannian manifolds. *Journal of Mathematical Imaging and Vision*, **50**, 32–52.

- Hong, Y., Singh, N., Kwitt, R., Vasconcelos, N. and Niethammer, M. (2016). Parametric regression on the Grassmannian. *IEEE Transactions on Pattern Analysis and Machine Intelligence*, **38**, 2284–2297.
- Kim, H. J., Adluru, N., Collins, M. D., Chung, M. K., Bendin, B. B., Johnson, S. C., Davidson, R. J. and Singh, V. (2014). Multivariate general linear models (MGLM) on Riemannian manifolds with applications to statistical analysis of diffusion weighted images. *2014 IEEE Conference on Computer Vision and Pattern Recognition*, 2705–2712.
- Mortici, C. (2012). Completely monotone functions and the Wallis ratio. *Applied Mathematics Letters*, **25**, 717–722.
- Steinke, F. and Hein, M. (2008). Non-parametric regression between manifolds. *Advances in Neural Information Processing Systems 21*.
- Steinke, F., Hein, M. and Schölkopf, B. (2010). Nonparametric regression between general Riemannian manifolds. *SIAM Journal on Imaging Sciences*, **3**, 527–563.
- Zhang, X., Shi, X., Sun, Y. and Cheng, L. (2019). Multivariate regression with gross errors on manifold-valued data. *IEEE Transactions on Pattern Analysis and Machine Intelligence*, **41**, 444–458.